INCORPORATION AND DECONTAMINATION PERFORMANCE OF MOLECULAR POLYOXOMETALES IN FIBROUS SUBSTRATES

A Dissertation
Presented to the Faculty of the Graduate School
of Cornell University
In Partial Fulfillment of the Requirements for the Degree of
Masters of Science

by
Nancy Elizabeth Allen
May 2013

Abstract

Combining unique fiber morphologies with new self-decontamination technologies can enhance chemical warfare agent and toxin degradation on textile substrates. Co-continuous electrospinning was used to fabricate nanofibrous cellulose acetate membranes with unique, grooved fiber morphology due to the selective dissolution of polyethylene oxide. The BET gas adsorption surface area of these grooved fibers was compared to the surface area of non-grooved electrospun cellulose acetate / polyethylene oxide fibers. A self-decontaminating polyoxometalate ($H_5PV_2Mo_{10}O_{40}$) was synthesized and characterized via Fourier transform infrared spectroscopy, x-ray diffraction, scanning electron microscopy, energy dispersive spectroscopy, and thermal gravimetric analysis. Both the grooved and non-grooved fibers, in addition to cotton, were functionalized with the catalytic molecular polyoxometalates (POMs) via covalent grafting to the substrate surfaces, and the POM-treated fibrous substrates were then exposed to methyl parathion, an organophosphate simulant of the chemical warfare agent (CWA) VX, in solution for 24 hours. The degradation of methyl parathion by the POM treated substrates was measured using high performance liquid chromatography, and the degradation performance of the substrates was compared and related to their properties and morphology. Relative to the non-grooved fibers, the creation of the grooved fiber morphology resulted in a significantly larger surface area for which the POMs to bind, and the amount of methyl parathion degradation over time was significantly enhanced. The grooved fiber morphology grafted with POMs degraded twice the amount of methyl parathion than the non-grooved fiber morphology. Cotton grafted with POMs was found to have the highest surface area and degraded the most methyl parathion. After 24 hours, the methyl parathion was completely

degraded by the POM-grafted cotton. POM catalytic oxidation and hydrolysis degradation mechanisms and degradation products were examined to better understand the efficacy of POM treated substrates, and results suggest the presence of moisture may have played a key role in greater methyl parathion degradation. This work may contribute in the future to the use of novel fiber morphologies in more breathable chemical protective apparel to achieve a greater amount CWA decontamination, protection, and comfort.

Biographical Sketch

Nancy Elizabeth Allen is currently a graduate student at Cornell University, (Ithaca, NY) studying Fiber Science & Apparel Design. Originally from Charleston, SC, she received her B.S. in Polymer and Fiber Chemistry at Clemson University (Clemson, SC) and worked as a color chemist for Milliken Chemical (Spartanburg, SC) prior to her admission at Cornell. Her research interests include textile chemistry, color chemistry, protective apparel, ergonomics, and chemistry in functional design.

To

William and Henry

Acknowledgements

Great thanks are extended to Dr. S. Kay Obendorf for her efforts as my advisor in the development of this project and for her valued guidance and expertise. Also, the help of Dr. Susan Ashdown, Dr. Jintu Fan, Dr. Dong Jin Woo, Laurie Lange, John Hunt, the CCMR staff of Cornell University has been much appreciated. I am very grateful for the financial support of the Department of Fiber Science & Apparel Design at Cornell University & the American Association of Textile Chemists and Colorists.

Also, special thanks are due to my family for their continued love and support while I pursue my research and to Dr. Phil Brown and Dr. Kate Stevens for their encouragement through the years.

Table of Contents

2. Introduction

Polyoxometalates (POMs) are heteropolyanions, which can be used to oxidize or hydrolyze chemical warfare agents. These reactions can degrade substances such as the organophosphate nerve gas VX into less harmful byproducts. When the oxidation reaction occurs, the POM is reduced. Oxygen or any oxidant in the system can then re-oxidize the POM to its original state; the self-decontaminating agent is regenerated to be used for multiple decontamination cycles (Ozer and Ferry, 2000).

POMs have been incorporated into fibers and fabrics such as polyacrylic, nylon, cotton, and polyurethane sponges in order to examine their catalytic self-decontamination of volatile organics, air toxins, and chemical warfare agents. POMs grafted to cotton and other cellulosic substrates have been examined for breathable protective performance apparel (Xu et al., 2000; Walker et al., 2003; Drechsler et al., 2009).

POMs such as $H_5PV_2Mo_{10}O_{40}$ have been prepared by Dr. Craig Hill of Emory University and can be incorporated into micro- or nano- electrospun fibers and film coatings for fabrics (Gall et al., 1996). 10-Molybdo-2-vanadophosphoric acid has been incorporated into cellulose substrates to degrade volatile organics and chemical warfare agents such as CEES (Xu et al., 2000; Hill et al., 2001; Drechsler et al., 2009).

The current approach to achieving enhanced methyl parathion degradation with POMs in grooved cellulose acetate nanofibers entailed the fabrication of the high surface area cellulose acetate membrane, its characterization, POM synthesis, the grafting of POMs to the cellulose acetate membrane, and the characterization and decontamination performance of the POM functionalized membranes.

3. Statement of Purpose

The overall objective of this work was to incorporate high loads of self-decontaminating compounds in semi-permeable, breathable, textile substrates to achieve their self-decontaminating performance. As part of this overall objective, many steps must take place in order to achieve this goal of enhanced decontamination. The raw material polyoxometalate (POM) $H_5PV_2Mo_{10}O_{40}$ was synthesized and characterized. A dual component cellulose acetate / polyethylene oxide polymer membrane was electrospun and characterized. Polyethylene oxide was selectively dissolved from the fibrous substrate in order to create high surface area grooved fiber morphology, and characterization of this process was performed to confirm the increased surface area. The self-decontaminating POM was grafted to both the treated and non-treated membranes as well as 100% cotton for comparison, and the self-decontamination performance was measured and analyzed. The purpose of this work is to develop new self-decontaminating materials for use in protective clothing.

4. Background and Justification

Ongoing global conflicts and the use of chemical weapons require the advancement of personal protective apparel. Developing technologies in protective apparel aim to reduce exposure to chemical warfare agents (CWAs) in liquid, vaporous, or particulate forms while maintaining personnel thermal comfort, breathability, and human performance. Microfibrous and nanofibrous functionalized, self-decontaminating membranes with engineered pore structures can be applied to protective apparel to prevent CWA penetration while allowing moisture vapor to be transported through the garment.

Current garments that protect against CWAs such as distilled mustard, lewisite, tabun, sarin, soman, and *O*-ethyl *S*-[2-(diisopropylamino) ethyl] methylphosphonothioate, a highly toxic nerve agent commonly known as VX, are mostly composed of bulky impermeable barrier materials that do not allow chemicals to penetrate through the garment, nor do they allow moisture, mainly in the form of perspiration, to escape (Bartelt-Hunt, 2008). As a result, these suits lack provisions for thermal comfort in extreme hot and cold environments and cannot be worn for extended periods of time. Their bulkiness reduces dexterity and functionality. After CWA exposure, current military suits that employ activated carbon must be decontaminated before doffing, and they are disposed of as hazardous waste to prevent further contamination. A breathable, self-decontaminating material would improve the functionality, performance, re-useability, and disposal of chemical protective garments.

4-1. Polyoxometalate Structure and Reactivity

Polyoxometalates are heteropolyanions, otherwise known as polymeric oxoanions, formed by the condensation of more than two different oxoanions. These negatively charged nanoclusters of oxide and transition metal ions in their highest oxidation state have the general formula of $XM_{12}O_{40}$. X can be Si^{4+} or P^{5+} etc, and M can be tungsten, molybdenum, vanadium and other metals (Misono, 1987). The substitution of one or more tungsten or molybdenum ions in the structure creates a mixed addenda POM (Hill and McCartha, 1995). It is thought that the metal ion (M) acts as the self-decontaminating component of the POM, while the X (phosphorus, silicon, aluminum, boron, cobalt, zinc, or iron) provides structural integrity (Hill et al., 2001). The oxoanions molybdenum (Mo),

tungsten (W), vanadium (V), niobium (Nb), and tantalum (Ta) are present as acidic elements in aqueous solutions and polymerize to form polyanions at low pH. In their free acid form, polyoxometalates are referred to as heteropoly or isopoly acids. POM free acids and their salts act as strong acids and have been widely used as acid catalysts and oxidation catalysts that yield better oxidation performance than hydrogen peroxide, ozone, and molecular oxygen when environmental profiles and efficiency of oxidation are taken into consideration (Misono, 1987). Vanadates, niobates, tantalates, molybdates, tungstates, and mixed addenda heteropolyanions make up the different classes of polyoxometalates. Mixed addenda polyanions can include molybdovanadates, tungstovanadates, niobotungstates, and molybdotungstates (Pope, 1983).

The majority of polyanions with tetrahedrally-coordinated heteroatoms have structures based on what is known as the Keggin anion (Pope, 1983). Among the many Keggin isomers, there are two main anion isomers classified as α- and β-$XM_{12}O_{40}$. The α-Keggin structure (α-$[XM_{12}O_{40}]^{n-}$) has overall symmetry and is based on a central XO_4 tetrahedron surrounded by twelve MO_6 octahedra arranged in four groups of three edge-shared octahedral, M_3O_{13} (Keggin, 1933; Pope, 1983). One of the most heavily researched mixed addenda POMs, $PMo_{10}V_2O_{40}^{5-}$ is a disubstituted α-Keggin complex with five distinct isomers (Hill and McCartha, 1995). Figures 1 and 2 display the particular structure of $H_5PV_2Mo_{10}O_{40}$ (Pope, 1983; Johnson and Hill, 1999; Arichi et al., 2010). $H_5PV_2Mo_{10}O_{40}$ is used commonly in homogeneous catalytic oxidation processes since vanadium is the most strongly oxidizing addenda element (Hill and McCartha, 1995).

There are five homogeneous modes through which polyoxometalates aid the oxidation of substrates. The process of the first and most common mode begins with the

direct oxidation of a substrate by the polyoxometalate. The reduced POM is then re-oxidized to its original state by any oxidant in the system (Kozhevnikov and Mateev, 1983; Neumann and Assael, 1988; Hill et al., 1993; Gall et al., 1994; Ozer and Ferry, 2000). This mode applies to the POM $H_5PV_2Mo_{10}O_{40}$ when oxidizing substrates such as aromatic and alkyl aromatic compounds in the liquid homogeneous phase via electron and oxygen transfer in what is known as a Mars-van Krevelen reaction. For example, cyclic dienes, alcohols, amines, and phenols undergo oxidative dehydrogenation, meaning there is an electron and proton transfer from the substrate P-H_2, to the polyoxometalate (Khenkin et al., 2001). Scheme 1 represents the oxydehydrogenation of the previously mentioned substrates (Khenkin et al., 2001). It is important to note that the substrates are not oxygenated, implying there is no oxygen transfer from the metal oxide (Khenkin et al., 2001). Figure 3 represents the rapid, reversible redox changes that classify these nanoparticles as catalytic and self-regenerating (Ozer and Ferry, 2000; Khenkin et al., 2001). In its second oxidation mechanism mode, the POM can act as a co-catalyst following the path of Wacker reaction homogeneous catalysis (Kozhevnikov and Mateev, 1983; Gall et al., 1994). In mode three, the POM acts to oxygenate the substrate (Hill and Brown, 1986; Gall et al., 1994). In mode 4, the POM acts as a photocatalyst, and in mode 5 the POM in its excited state oxidizes the substrate directly (Hill et al., 1993; Gall et al., 1994).

In the first mode, the presence of water plays a significant role in POM catalytic oxidation in non-aqueous or non-polar environments. As water content increases, the rate of catalytic oxidation increases. Therefore, $H_5PV_2Mo_{10}O_{40}$, a POM in its hydrated form, is preferable to use in order to achieve greater catalytic oxidation of chemical warfare agents

and their simulants (Gall et al., 1994). When using this hydrated POM via mode one catalysis, only the vanadiums (not the molybdenums) are reduced when the POM oxidizes a substrate (Gall et al., 1994).

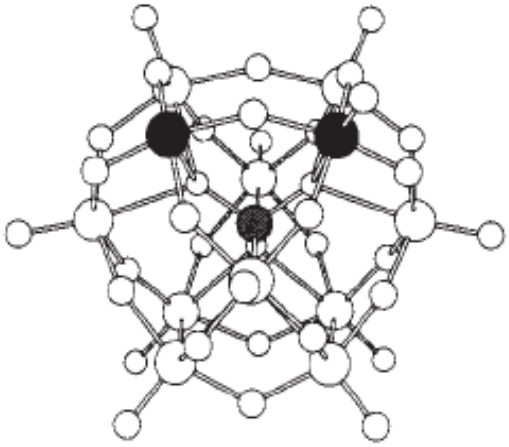

Figure 1: Structure of $H_5PV_2Mo_{10}O_{40}$ with the central phosphorous heteroatom shaded grey and the two vanadium atoms shaded black (Johnson and Hill, 1999)

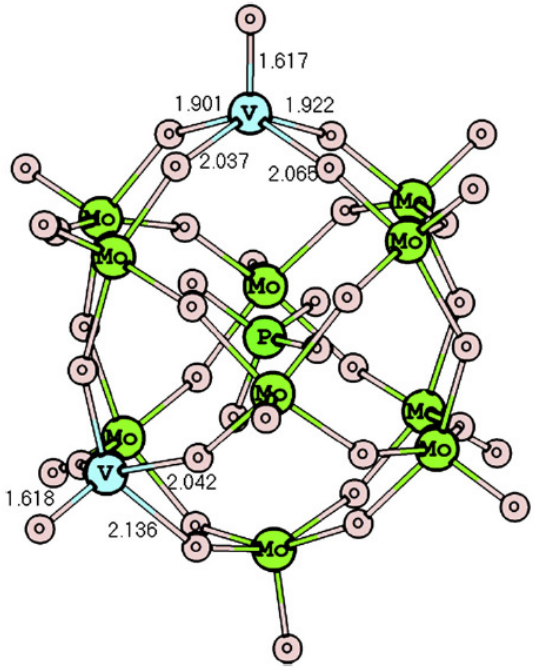

Figure 2: PM6 optimal geometry of Keggin unit containing two vanadium atoms (Arichi et al., 2010)

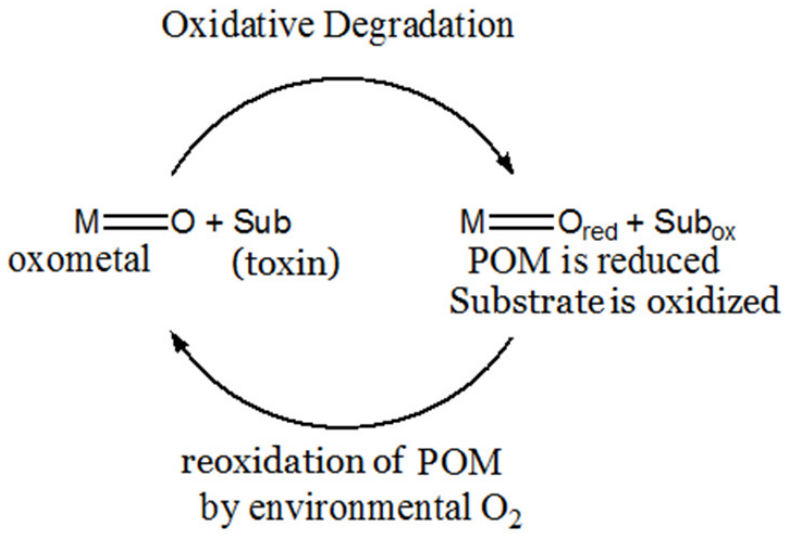

Figure 3: Catalytic cycle of polyoxometalate nanoparticles (Ozer and Ferry, 2000)

Scheme 1: The oxidative dehydrogenation of aromatic and alkyl aromatic substrates (Khenkin et al., 2001)

$$P\text{-}H_2 + POM_{ox} \longrightarrow P + 2H^+ + POM_{red}$$

$$2H^+ + POM_{red} + 1/2O_2 \longrightarrow POM_{ox} + H_2O$$

A simulant of CWA VX, methyl parathion (O, O-dimethyl O-p-nitrophenyl phosphorothioate) is thought to be catalytically oxidized by the POM $H_5PV_2Mo_{10}O_{40}$. This can be likened to the degradation mechanism of methyl parathion via TiO_2, which is shown in Scheme 2 (Senthilnathan and Philip, 2010). TiO_2 acts as a photocatalyst and requires UV light to catalytically oxidize the toxin; whereas, $H_5PV_2Mo_{10}O_{40}$ requires no UV light to degrade methyl parathion. In the oxidation reaction with TiO_2 the main degradation products of methyl parathion are methyl paraoxon, O,O,O-trimethyl phosphoric thiourate, and p-nitrophenol (Senthilnathan and Philip, 2010). Given the similarity in mechanisms,

the degradation products of methyl parathion when catalytically oxidized by $H_5PV_2Mo_{10}O_{40}$ were expected to be the same.

Scheme 2: Possible degradation pathway of methyl parathion in coated TiO_2 (Senthilnathan and Philip, 2010)

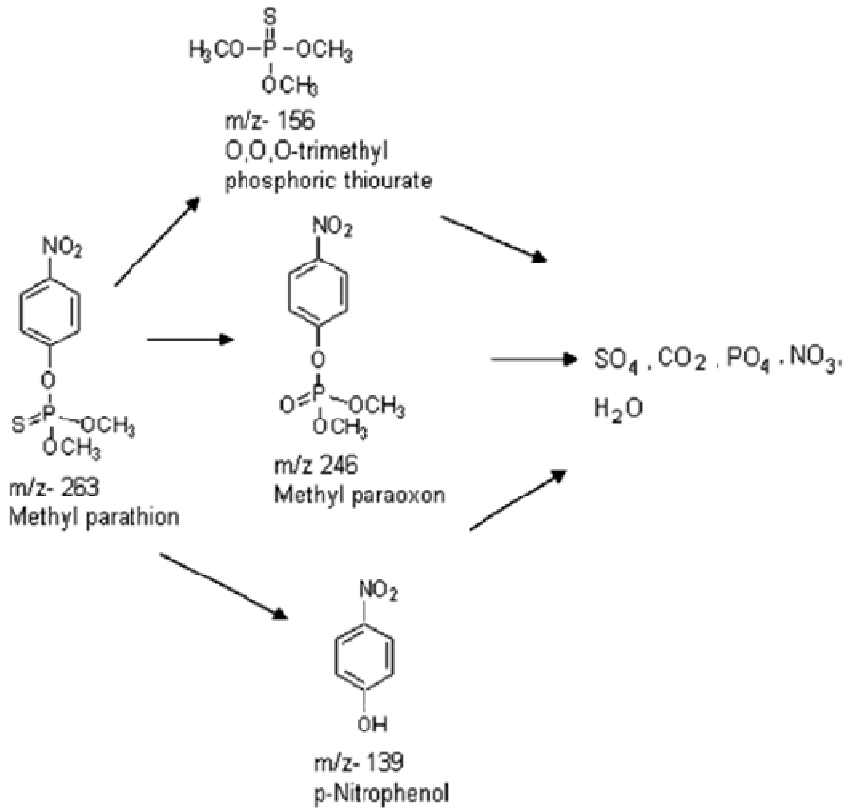

A second mechanism of POM degradation is hydrolysis. POMs such as $H_5PV_2Mo_{10}O_{40}$ have strong Brønsted acid strength, akin to that of sulfuric acid. In the presence of water, the protons of the POM can disassociate more readily and become free to interact with the P-O linkage of the organophosphate methyl parathion (Morrow and Trogler, 1989; Sharmila et al., 1989; Tian et al., 2010). This leads to the cleavage of the

aryl ester P-O linkage via nucleophilic displacement at the phosphorus thus resulting in the degradation of methyl parathion into diethylthiophosphate and p-nitrophenol as seen in Scheme 3 (Fee, 2000; Metcalf, 2000; Morrow and Trogler, 1989). In an anaerobic environment, the hydrolysis of methyl parathion proceeds as shown in Scheme 4 where the nitro group on the methyl parathion is reduced to an amine (Fee, 2000).

Scheme 3: Hydrolysis of methyl parathion in aerobic conditions (Fee, 2000; Metcalf, 2000; Morrow and Trogler, 1989)

$$(C_2H_5O)_2P(S)OC_6H_4NO_2 + H_2O \rightarrow HOC_6H_4NO_2 + (C_2H_5O)_2P(S)OH$$

Scheme 4: Hydrolysis of methyl parathion in anaerobic conditions (Fee, 2000)

$$(C_2H_5O)_2P(S)OC_6H_4NO_2 + 6\ H \rightarrow (C_2H_5O)_2P(S)OC_6H_4NH_2 + 2\ H_2O$$

It has been shown that both in the liquid and gas homogeneous phases as well as when grafted to the surface of fabrics such as such as polyacrylic, nylon, cotton, other cellulosic fibers, polyester, polyacrylonitrile, polyvinylidene, polyolefin, polyurethane, polytetrafluoroethylene, carbon cloth, other carbon-based fabrics such as electrospun Estane® microfibers, and combinations thereof, polyoxometalates can decontaminate volatile organics and chemical warfare agents such as the thioether mustard analog (HD), the CWA simulant 2-chloroethylethyl sulfide (CEES), and multiple organophosphates such as the nerve agent known as VX (Lissel and Jansen, 1992; Gall et al., 1994; Johnson and Hill, 1999; Ozer and Ferry, 2000; Xu et al., 2000; Hill et al., 2001; Walker et al., 2003; Drechsler et al., 2009; Mizrahi et al., 2010).

4-2. POM Functionalized Microporous Fibrous Substrates

POMs have been incorporated into electrospun, microporous, nanofibrous cellulose acetate membranes in order to increase the number of active POM binding sites on fibers. This increase in surface area has enabled increased catalytic decontamination of volatile organics such as acetaldehyde and 1-propanethiol and CWAs such as sulfur mustard and VX due to the large fiber surface area (Xu et al., 2000, Drechsler et al., 2009, Hill et al., 2001). The background to this technology includes understanding how to fabricate high surface area cellulose acetate membranes, its characterization, POM synthesis, the grafting of POMs to the cellulose acetate membrane, and the characterization of the POM functionalized membranes.

4-3. Fabrication & Characterization of High Surface Area Cellulose Membranes

In order to electrospin, a polymer solution must be agitated at room temperature until full dissolution is achieved. The polymer solution is poured into an electrospinning reservoir. A stainless steel electrode is then placed in the solution and connected to a power supply with a grounded counter electrode connected to an aluminum foil fiber collection plate that can be placed at a specified distance from the electrode. Once the electrode reaches critical voltage, electrostatic forces overcome the surface tension of the solution, and a jet is ejected and accelerated to the upper aluminium foil collection plate due to the electric field generated between the electrode and counter electrode. The jet splits into fiber filaments due to electrostatic instability forming interconnected fibrous membranes. These filaments solidify once the solvent evaporates and can be removed from the aluminum collector and dried under vacuum. (Doshi and Reneker, 1995).

The pore size, pore size distribution, adsorption, penetration, fiber size, fiber morphology, and surface area of these membranes can be measured using a porometer, a scanning electron microscope (SEM), and a gas adsorption technique known as BET. This technique measures the physical adsorption of gas molecules on a solid surface in order to analyze the surface area of a material. The measurement of additional mechanical and thermal properties also helps to characterize the composition of the membranes. Dixit et al., 2009 demonstrated that electrospun regenerated cellulose nanofiber membranes can be loaded with self-decontaminating compounds, such as saponin, which show good performance in degrading biological agents with potential applications in protective apparel.

4-3-1. Co-continuous Polymer Structures

Woo, 2012, used co-continuous electrospun fibers to exhibit that fiber morphology can influence the diffusion of chemical warfare agents and other toxins in order to improve self-decontamination technologies on fiber substrates. He showed that fibers that are monoaxially spun with the active self-decontaminating technology can limit the efficiency of decontamination. This is a result of the technologies being contained within the fiber and unavailable to surface reactions that would enhance toxin degradation (McCann et al., 2005). Co-continuous electrospinning is a process that employs phase separation of a solution to spin a blend of polymers. An interconnected, microporous structure with deep pores, grooves, and channels in the fiber is created by selective dissolution, where one of the polymers is removed from the co-continuous blend post-electrospinning (Tang et al., 2008). These pores, grooves, and channels provide more surface area on the fibers for

which a decontaminating agent, such as POMs, can bind and enhance the surface reaction efficiency of the fibers (Tang et al., 2008; Zhang et al., 2010; Nguyen et al., 2010). Tang and his colleagues (2008) showed how acetone could be used to selectively dissolve cellulose acetate from a cellulose acetate / polyurethane co-continuously spun polymer fiber blend in order to create a porous polyurethane fiber.

Following Tang's example, Woo, 2012, blended two polymers (cellulose acetate and polyethylene oxide) in a specific ratio of two solvents (acetone and acetonitrile) and then used this uniform dispersion to co-continuously electrospin a high surface area nanochannelled fibrous cellulosic membrane. The solubility parameters of the polymers were critical to achieving this unique fiber morphology since optimal co-continuous phase formation occurs when the polymer solution is near the interface between a 1-phase-system and 2-phase-system as represented by the solid line in the solubility diagram (Figure 6). Cellulose acetate was chosen as a polymer since it is soluble in acetone and acetonitrile, and polyethylene oxide was chosen because it is only partially soluble in acetone and can be extracted from the co-continuous polymer matrix via hot water dissolution. Partial solubility of polyethylene oxide was desired to achieve optimal phase formation. After testing several formulations of these four components, Woo achieved optimal nanochannels and high surface area fibers by electrospinning a solution composed of 15% dual component polymer (60% cellulose acetate [CA], 40% polyethylene oxide [PEO]) and 85% dual component solvent (60% acetonitrile, 40% acetone) and then performing a hot water Soxhlet extraction on the fibers for several hours. The condensed boiling water extracted the polyethylene oxide from the fibers. After extraction, the fibers were vacuum dried. The resulting fibers were composed of cellulose acetate with grooves or channels

created where the polyethylene oxide was originally present. A schematic of this process can be seen in Figure 4, and an SEM of the resulting fiber is shown in Figure 5. This blend is shown on a solubility diagram (Figure 6) which Woo used to determine the optimal solubility for achieving this unique channeled co-continuous fiber morphology.

Figure 4: Co-continuous fiber formation using cellulose acetate (CA) and polyethylene oxide (PEO)

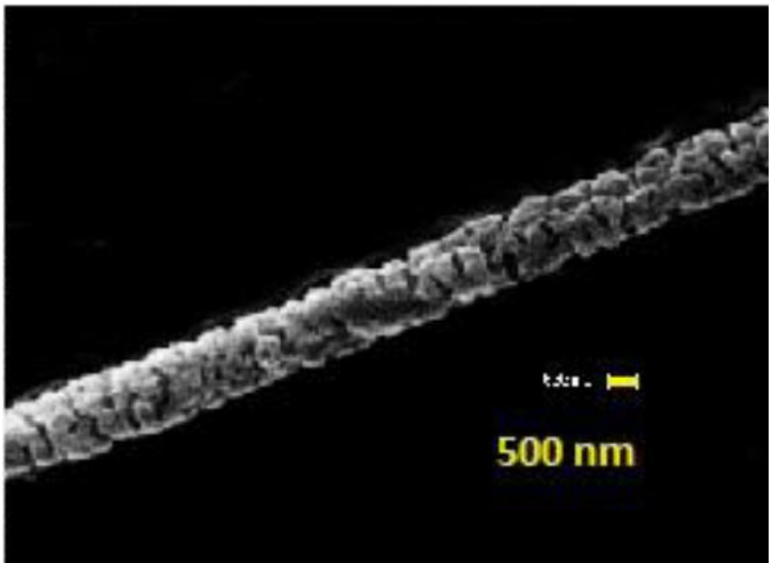

Figure 5: SEM of nanochanneled cellulose acetate / PEO fiber morphology (Woo, 2012)

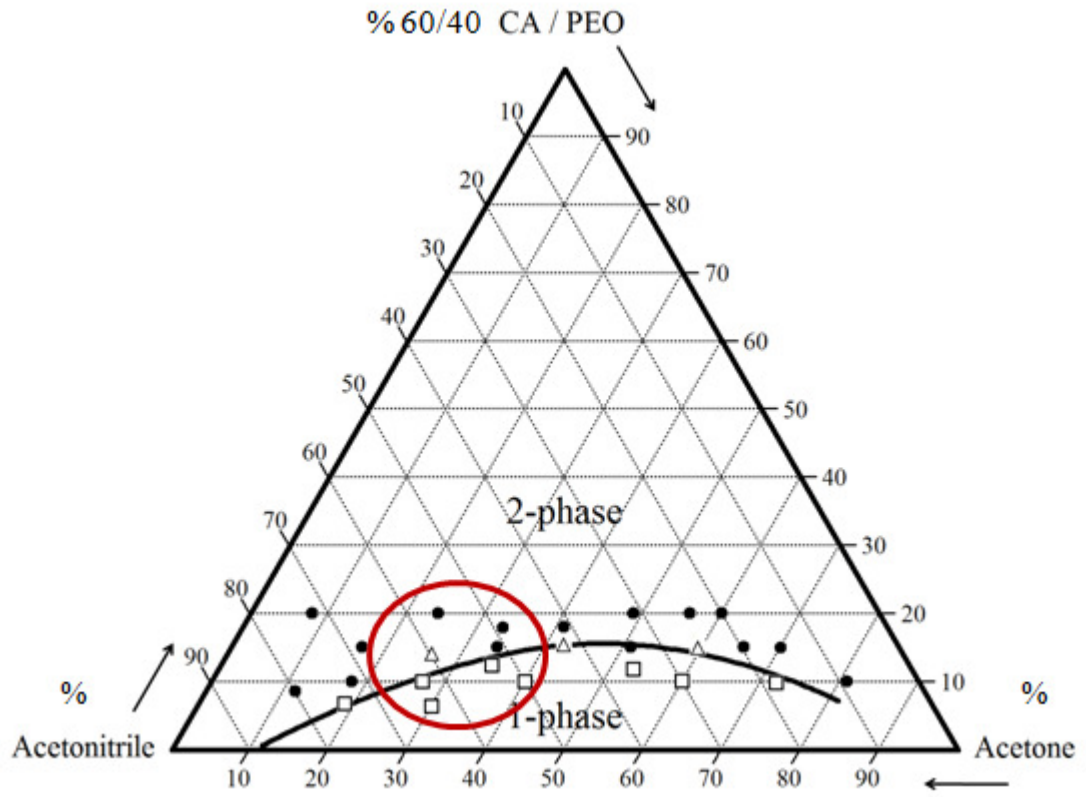

Figure 6: Solubility Diagram of Cellulose Acetate / Polyethylene Oxide blends in Acetone and Acetonitrile (Woo, 2012)

4-3-2. Solubility Parameters

It is necessary to examine the dissolution properties of the dual polymer / dual solvent electrospinning solution more closely in order to understand the unique fiber morphology this formulation creates. While cellulose acetate is soluble due to its polarity (acetyl content = 39.8%, degree of substitution = 2.45) in both acetone and acetonitrile, polyethylene oxide, which is less polar than cellulose acetate, is not fully soluble in either solvent at ambient conditions (Vallejos et al., 2012). At temperatures above 40°C, polyethylene oxide becomes more soluble in acetone. Neither solvent has a high hydrogen bonding strength. Additional information regarding the physical properties and solubility

of the polymers and solvents can be found in Tables 1 and 2 in Section 6-2-3-1. When combined at certain ratios, the partially immiscible polymer mixture forms a uniform dispersion in the dual component (60/40 acetonitrile to acetone) solvent only after being agitated at high speeds for 1-8 h in a 40°C warm water bath. After electrospinning, one of the polymers can be extracted successfully due to its original partial immiscibility leaving behind a co-continuous fiber composed of the polymer that was not extracted. The partial immiscibility of polyethylene oxide in acetone and acetonitrile due to the lower polarity of PEO is advantageous in the creation of a co-continuous fiber morphology. It enables polyethylene oxide to be extracted after electrospinning leaving behind a co-continuous cellulose acetate fiber. It is essential to understand these solubility parameters in order to achieve co-continuous fiber morphology and fabricate high surface area fibers.

4-4. Polyoxometalate Synthesis

Heteropolymolybdovanadates such as the free acid of the anion $[PMo_{10}V_2O_{40}]^{5-}$ referred to as 10-molybdo-2-vanadophosphoric acid ($H_5PV_2Mo_{10}O_{40}$) can be synthesized via a known process involving the reaction of sodium metavanadate ($NaVO_3$) with disodium phosphate (Na_2HPO_4) and the resulting reaction of the compound with concentrated sulfuric acid and sodium molybdate (Na_2MoO_4) in an oxygen containing solvent such as ethyl ether, ethyl alcohol, methanol, ethyl acetate, dimethyl sulfoxides, or tetrahydrofuran. It is necessary to purify the acids to obtain the correct stoichiometry. After extraction, the resulting compound appears as reddish orange crystals (Tsigdinos and Hallada, 1967). The microscopically self-assembled cubic crystals are expected to be on the scale of 70 μm and are formed from the aggregation of nano-scale building blocks

(Arichi et al., 2010). The particles can be characterized via x-ray diffraction (XRD), Fourier transform infrared spectroscopy (FTIR), scanning electron microscopy (SEM), and energy dispersive spectroscopy (EDS) (Pettersen et al., 1994, Selling et al., 1994, Arichi et al., 2010, Nielsen et al., 2010). Figure 7 shows an example of an SEM image of microscale $H_5PV_2Mo_{10}O_{40}$ after synthesis (Nielsen et al., 2010).

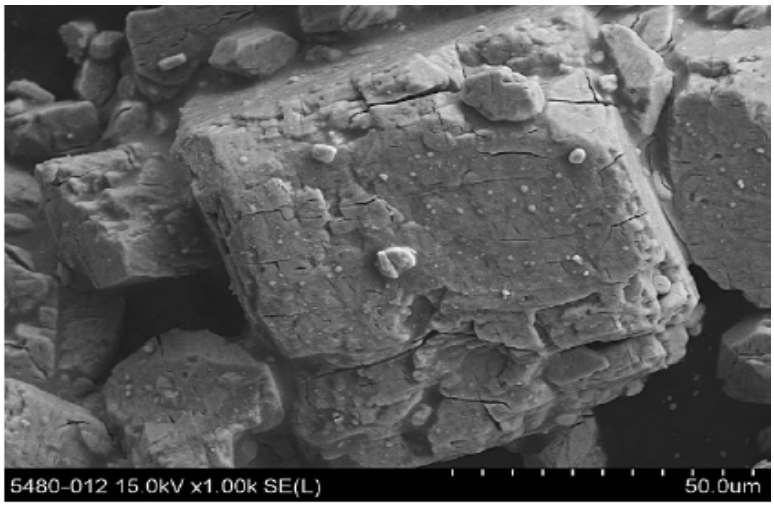

Figure 7: SEM Image of self-organized $H_5PV_2Mo_{10}O_{40}$ material (Nielsen et al., 2010)

4-5. Grafting POMs to Cellulose Substrates

Drechsler et al., 2009 functionalized polymers with reactive species such as polyoxometalates by creating reactive oxygen species (ROS) on a polyurethane sponge via plasma treatment. The ROSs were then reacted with polyurethane and diisocyanate in the presence of argon and toluene creating isocyanate and silyl groups on the surface of the polymer that provided active binding sites for POMs. The POMs were grafted to the surface of the polymer surface in the presence of argon and tetrahydrofuran at room temperature for 24 h. A similar procedure was used by Tan and Obendorf, 2005 to create

grafting sites on a polyurethane membrane for poly(ethylene glycol). The reaction was performed under a nitrogen purge in the presence of a tin (II) catalyst, a toluene solvent, and a swelling agent (Tan and Obendorf, 2005). This process can be modified slightly to graft polyoxometalates to cellulose membrane substrates. The limit to the amount of POM grafted to the surface of the membrane is the number of polyurethane functionalized reaction sites on the surface of the cellulosic fibrous surface. A suggested concentration range on cellulosic fibers is 0.1-20% by weight of POM on the fabric surface (Hill et al., 2001).

4-6. Characterization of POM Functionalized Substrates

Schreuder-Gibson et al. (2002) developed a method for incorporating 10-molybdo-2-vanadophosphoric acid into electrospun fibers by dissolving POMs reacted with activated carbon or nano metal oxides in solutions of polyurethane and tetrahydrofuran (THF) in order to test their ability to destruct and absorb toxic organic compounds such as CEES. The structural effects upon moisture transport, air convection, aerosol filtration, porosity, tensile strength, and enhanced chemical activity of these membranes were measured using a variety of techniques (Schreuder-Gibson et al., 2002). Figure 8 shows the SEM images of an electrospun fiber mat used to incorporate CWA catalysts for protective clothing (Xu et al., 2000; Schreuder-Gibson et al., 2002; Walker et al., 2003).

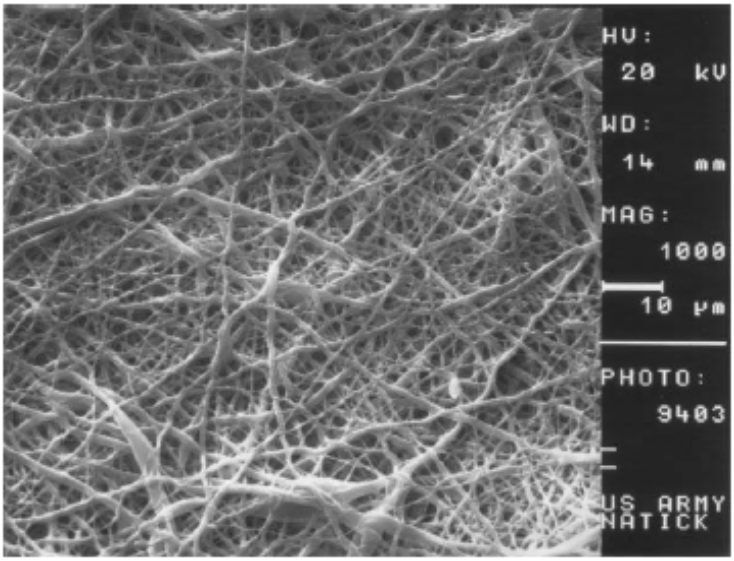

Figure 8: Electrospun fiber mat for incorporating CWA catalysts (Walker et al., 2003)

FTIR spectral analysis can be used to confirm the elemental composition of the membrane and the presence of the POM. Surface area measurements of the membrane can be made using BET nitrogen adsorption (Xu et al., 2000). Liquid chromatography-mass spectroscopy (LC/MS) can be used to measure the decomposition of methyl parathion (Walker et al., 2003). Pore size and pore size distribution of the membrane can be determined using a porometer and SEM images (Schreuder-Gibson et al., 2002). Since these membranes would serve as nanofiber layers in laminates within protective clothing, their ability to wick perspiration from the garment is essential (Schreuder-Gibson et al., 2002). Analysis to assess the breathability of the membranes and the water vapor transmission rate is needed in future experiments. Statistical analyses can help to determine overall trends resulting from the surface modification of the membrane with POMs and their degradation of methyl parathion.

4. Hypotheses

By using channeled cellulose acetate nanofibers, the surface area of traditional microporous nanofibrous cellulose acetate membranes will be increased providing more active sites to which the POMs will bind. This increase in POM active sites will enhance the catalytic degradation performance of methyl parathion, an organophosphate simulant of the chemical warfare agent (CWA) VX.

5. Materials & Methodology

6-1. Materials

Cellulose acetate (M_n 30,000) in powder form (180955) and poly(ethylene oxide) (M_v 200,000) (181994) were obtained from Sigma-Aldrich (St. Louis, MO) in addition to the solvents acetonitrile HPLC grade (AX0145-1) from EMD Chemicals, Inc (Gibbstown, NJ) and acetone (2440-16) from Mallinckrodt Chemicals (Phillipsburg, NJ) for electrospinning. BD Sterifill SCF 5-mL plastic syringes (Franklin Lakes, NJ) and a Harvard Apparatus PHD ULTRA electrospinning device (Holliston, MA) in combination with a Gamma High Voltage Research voltage source (Ormond Beach, FL) were used to fabricate the fibrous membranes.

100% Cotton swatches (Style 400U Unbleached desized Cotton Print Cloth) were obtained from Testfabrics, Inc (USA) and cut into 5 inch by 5 inch swatches.

$H_5PV_2Mo_{10}O_{40}$ was synthesized using sodium molybdate dehydrate from EMD Chemicals, Inc (EM-SX0650-2) (Phillipsburg, NJ), sodium metavanadate from Sigma-Aldrich (72060) (St. Louis, MO), sodium phosphate dibasic from Sigma-Aldrich (S0876)

(St. Louis, MO), 0.5 N sulfuric acid (38295) from Sigma-Aldrich Fluka Analytical (St. Louis, MO), and methanol HPLC grade (34860) from Sigma-Aldrich (St. Louis, MO).

In order to graft the membranes with the polyoxometalates, Tin (II) 2-ethylhexanoate (S3252) and hexamethyl diisocyanate (HMDI) (52649) were obtained from Sigma-Aldrich (St. Louis, MO). Toluene (FW-92.14, Lot: B46B20) was also obtained from Mallinckrodt Chemicals (Phillipsburg, NJ).

The pesticide, methyl parathion (PS-94), and its degradation product, methyl paraoxon otherwise known as dimethyl-p-nitrophenylphosphate (PS-613) were purchased from Chem Service Incorporated (West Chester, PA). The methyl parathion degradation product p-nitrophenol (1048) was purchased from Sigma-Aldrich Fluka Analytical (St. Louis, MO).

Silanization of all glassware was done to reduce the adsorption of methyl parathion and its biproducts onto the surface of the glassware to keep subtle samples protected against the reactive effect of OH sites on the glassware. Silanization was done by coating and rinsing glassware with 5% (v/v) dimethyldichlorosilane in toluene for 10-15 seconds followed by two rinses with pure toluene and three rinses with methanol (Hong et al., 2001). The glassware was then oven dried. Dimethyldichlorosilane (440272) was purchased from Sigma-Aldrich (St. Louis, MO).

6-2. Methodology

6-2-1. $H_5PV_2Mo_{10}O_{40}$ Polyoxometalate Synthesis

In order to synthesize the $H_5PV_2Mo_{10}O_{40}$ POM, a sodium metavanadate solution was made by dissolving 24.4 g of $NaVO_3$ in 100 mL of boiling deionized water. After

complete dissolution, 5 mL of sulfuric acid was added. This solution was then cooled to room temperature. A sodium phosphate dibasic solution was made by slowly adding 7.1 g of Na_2HPO_4 to 100 mL of deionized water stirring at a high speed on a stir plate with a low and high setting to ensure complete dissolution. A sodium molybdate dihydrate solution was then made by dissolving 121 g of $Na_2MoO_4 \cdot 2H_2O$ in 200 mL of deionized water stirring at a high speed. The cooled sodium metavanadate solution was then added to the sodium dibasic solution while stirring at a high speed. These combined solutions were then added to the sodium molybdate dihydrate solution while stirring at a high speed. Then, 200 mL of 50 % sulfuric acid were added very slowly while the solution stirred vigorously. The addition of the acid raised the temperature of the solution significantly making slow addition of the acid imperative. Earlier studies on the synthesis of this compound recommended 85 mL of sulfuric acid or greater in order to achieve a weakly acidic pH. The slow addition of 200 mL of sulfuric acid achieved a pH of 3.79 which was measured once an hour for 4 h as the solution cooled to ensure pH stability. This cooled solution of 10-molybdo-2-vanadophosphoric acid was extracted with an excess (more than 500 mL) of methanol using a vacuum filter and flask as seen in Figure 9. The resulting precipitate was then dissolved in approximately 300 mL of water while stirring at a high speed. This solution was then placed over 50% sulfuric acid in a vacuum oven held at room temperature to enable the polyoxometalate 10-molybdo-2-vanadophosphoric acid to precipitate.

Extraction of 10-molybdo-2-vanadophosphoric acid with an excess of methanol in a vacuum filter flask

Precipitate that results from the extraction

Dissolved precipitate in deionized water precipitating over 50% sulfuric acid under vacuum

Figure 9: The extraction and precipitation of $H_5PV_2Mo_{10}O_{40}$

6-2-2. Characterization of Polyoxometalate particles

After synthesis, the particles were characterized via several of the methods established in the literature including x-ray diffraction (XRD), Fourier transform infrared spectroscopy (FT-IR), and scanning electron microscopy (SEM) (Pettersen et al., 1994; Selling et al., 1994; Arichi et al., 2010; Nielsen et al., 2010).

6-2-2-1. Fourier Transform Infrared Spectroscopy

The resulting particles were characterized first by Fourier transform infrared spectroscopy (FTIR) using a Nicolet Magna-IR 560 Spectrometer. In this technique infrared radiation is passed through the sample whether it is a solid on the mounting stage or a liquid held on a Teflon® holder. The resulting spectrum represents the molecular absorption and transmission of the sample. This resulting signature is unique to the molecular composition being tested. The size of the peaks is directly related to the amount of material present in the sample. Figure 10 illustrates this technique (Smith, 2011).

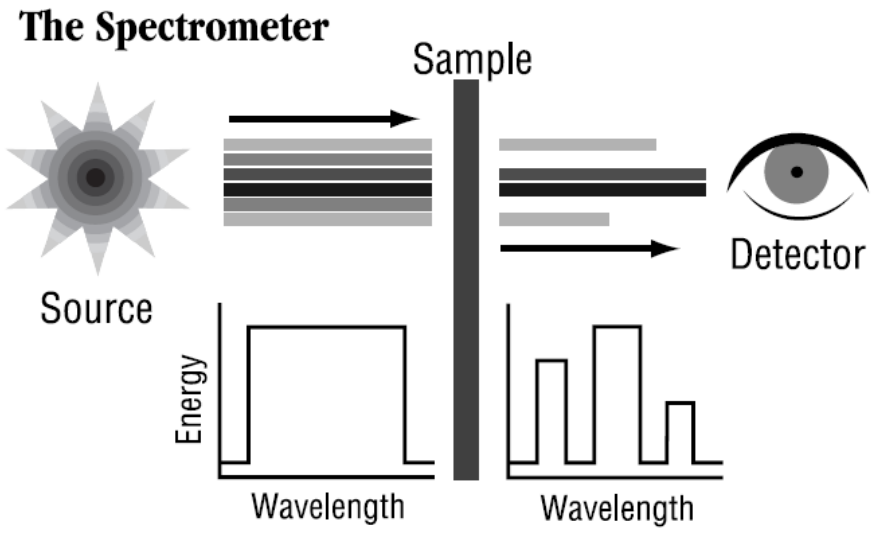

Figure 10: FTIR Molecular Absorption and Transmission (Smith, 2011)

A background spectrum was first measured on the instrument with no sample held in place in order to remove all instrumental characteristics from the standard spectrum and to provide a relative scale for the absorption intensity. Then the sample was placed on the platform ensuring good contact to eliminate air between the sample and the crystal, and the molecular absorption was measured. This procedure was repeated multiple times for different samples using the same background spectrum for each in order to analyze and identify changes in the molecular absorption signature.

The FTIR absorbance spectrum of $H_5PV_2Mo_{10}O_{40}$ was compared to the percent transmission FTIR spectrum found for this POM in the literature as seen in Figure 11 with characteristic peaks at 784 cm^{-1}, 958 cm^{-1}, 1057 cm^{-1}, 1618 cm^{-1}, 3422 cm^{-1} (Arichi et al., 2010).

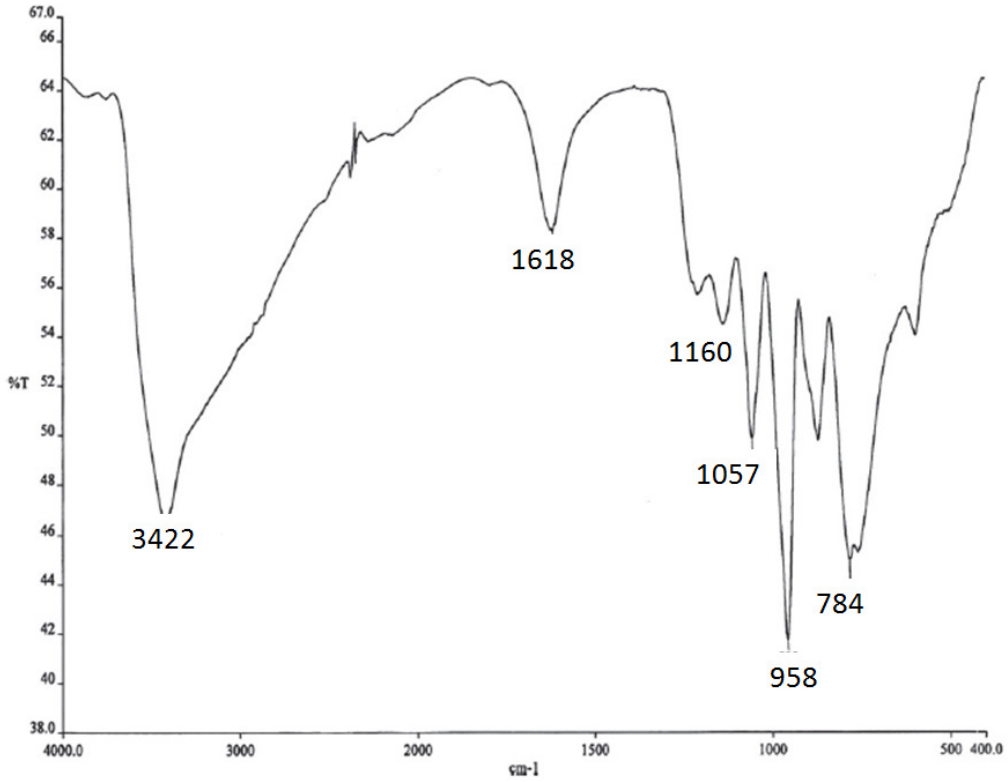

Figure 11: The FTIR spectrum of $H_5PV_2Mo_{10}O_{40}$ (Arichi et al., 2010)

6-2-2-2. X-ray Diffraction

X-ray diffraction (XRD) is an analytical technique used to identify a chemical compound by measuring the distances between the crystalline lattice spacings. Peaks seen at low two theta angles indicate large lattice spacings, while peaks at higher two theta angles indicate smaller lattice spacings. A Scintag Theta-Theta Diffractometer with a germanium detector was used to conduct this analysis. The POM powder sample was ground to a small, uniform size and was then mounted on an indented plate, and the powder was smoothed and flattened as much as possible. A line source of 1 x 10 mm was used, and the region hit by the x-ray beam was controlled by using slits at 0.3 mm (diffracted beam slit) and 0.5 mm (scatter slit) on the source. These slits were used to balance the resolution and intensity of the diffraction peaks in order to achieve high

resolution using lower intensities. The theta angle, i.e. the germanium detector position, was at 0° when the mounted sample was horizontally aligned, and the vernier scale detector angle was noted as 17.5°. The operating conditions of the instrument were set at a voltage of 45 kV and a current of 40 mA. A low to high angle continuous scan was made at a rate of 3° per minute (0.02° step size) within the range of 5° – 60° as determined from the literature (Popa et al., 2006; Arichi et al., 2010). The resulting peaks were compared to XRD patterns in the JADE software XRD library as well as the XRD results found in literature as seen in Figure 12 (Arichi et al., 2010).

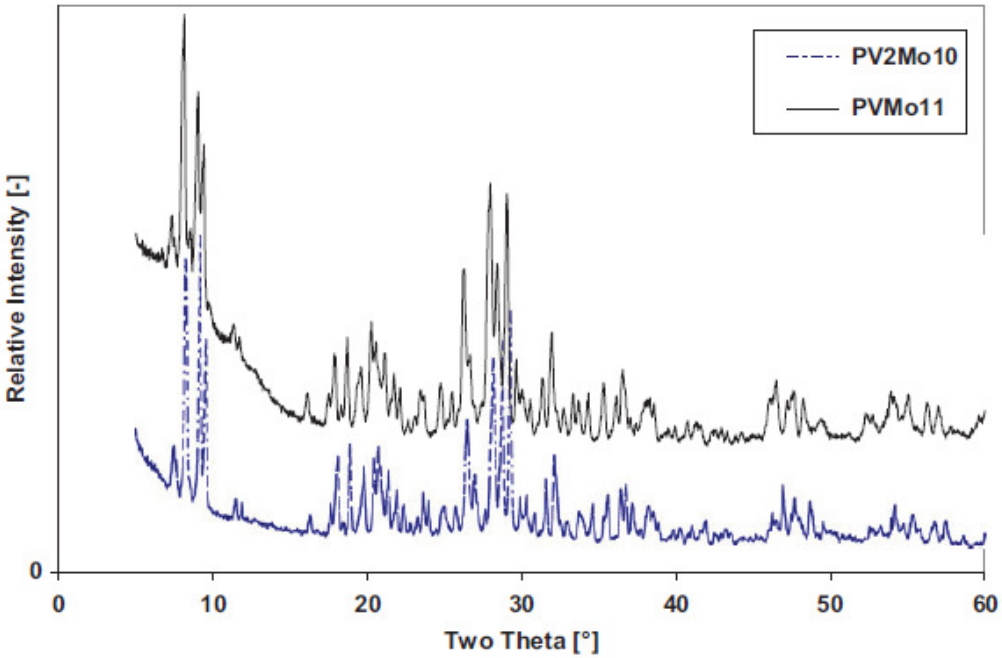

Figure 12: The XRD pattern of $H_5PV_2Mo_{10}O_{40}$ (Arichi et al., 2010)

6-2-2-3. Scanning Electron Microscopy

Scanning electron microscopy (SEM) on a Leica 440 (Leica Microsystems, Wetzlar, Germany) was used to analyze the morphology and size of the $H_5PV_2Mo_{10}O_{40}$ particles. In this technique an electron beam of energy of 0.2 keV – 40 keV is

thermionically emitted from a filament fitted within an electron gun. The filament is a loop of tungsten that functions as a cathode. The electron beam is focused by one or two condenser lenses to a spot 0.4 nm – 5 nm in diameter. As a voltage is applied to the tungsten loop cathode, it heats, and the anode forms powerful attractive forces for the electrons. The electrons then accelerate towards the anode while some accelerate past the anode moving down the column to the sample. In the final lens, the electron beam passes through pairs of scanning coils or pairs of deflector plates in the electron column. The final lens deflects the beam in the x and y axes so that it scans in a faster fashion, similar to the technique of image capture and reconstruction used for achieving television images, over a rectangular area of the sample surface. As a result, an image is generated (Goldstein, 1981). The voltage, position, contrast, focus, brightness, and magnification can be adjusted to obtain an optimal image. Higher voltage results in a higher resolution image (Echlin, 2009). Therefore, the clearest images were obtained using a voltage of 25 keV. Image J analysis was used to determine the size of the particles. It should be noted that before the particles were examined using the SEM, that the particle samples were mounted onto an SEM sample peg using double sided tape and then sputter coated with palladium and gold in order to make the samples conductive.

6-2-2-4. X-ray Microanalysis

There are two types of detectors for x-ray microanalysis that were used to analyze the POM nanoparticles. Energy dispersive x-ray spectroscopy (EDS), which measures the energy of the x-rays, and wavelength dispersive x-ray spectroscopy (WDS), which measures the wavelengths of the x-rays (Echlin, 2009). These techniques were used to

identify the composition of the synthesized compound and confirm that each element of $H_5PV_2Mo_{10}O_{40}$ was present.

Using equation 1 below, where E is the energy of the x-ray photon, h is Planks's constant 6.6262 x 10^{-34} JxS, λ is the wavelength of the x-ray photon, and c is the speed of light 3.0 x 10^8 m/s.

$$E = \frac{hc}{\lambda} \quad [1]$$

The equation shows that energy is inversely related to the wavelength. In the technique the wavelengths of the x-rays are separated with a crystal, which diffracts x-rays of certain wavelengths onto a detector. The x-rays enter the crystal and are scattered by the electrons. Each element present in the compound emits x-rays of particular wavelengths that are characteristic only for that element. Thus, the presence of certain elements can be established in the sample resulting in an element map where each of the elements is represented by a different color. The particle samples were mounted onto an SEM sample peg using double sided tape and then sputter coated with palladium and gold in order to make the samples conductive.

6-2-2-4-1. Energy-Dispersive X-ray Spectroscopy

Energy dispersive x-ray spectroscopy (EDS), which measures the energy of x-rays, was conducted using a JEOL JXA-8900R WD/ED Combined Microanalyzer instrument. This technique is achieved when a high-energy beam of charged particles (in this case electrons) is focused into the sample being studied. The incident beam excites an electron in an inner shell of the sample causing that electron to be ejected from the shell. This is

known as the critical excitation potential which is individual to each element. Once reached, electrons will be removed from the k-shell. Reaching this point creates an electron hole, which is then filled by an electron from an outer, higher-energy shell. The difference in energy between the higher-energy shell and the lower energy shell is released in the form of an x-ray. It is the number and energy of the x-rays emitted from the sample that are measured (Goldstein, 1981). Figure 13 illustrates this phenomenon. The energy of the x-rays is characteristic of the difference in energy between the two shells, and of the atomic structure of the element from which the electrons were emitted. This allows the elemental composition of the specimen to be measured (Goldstein, 1981).

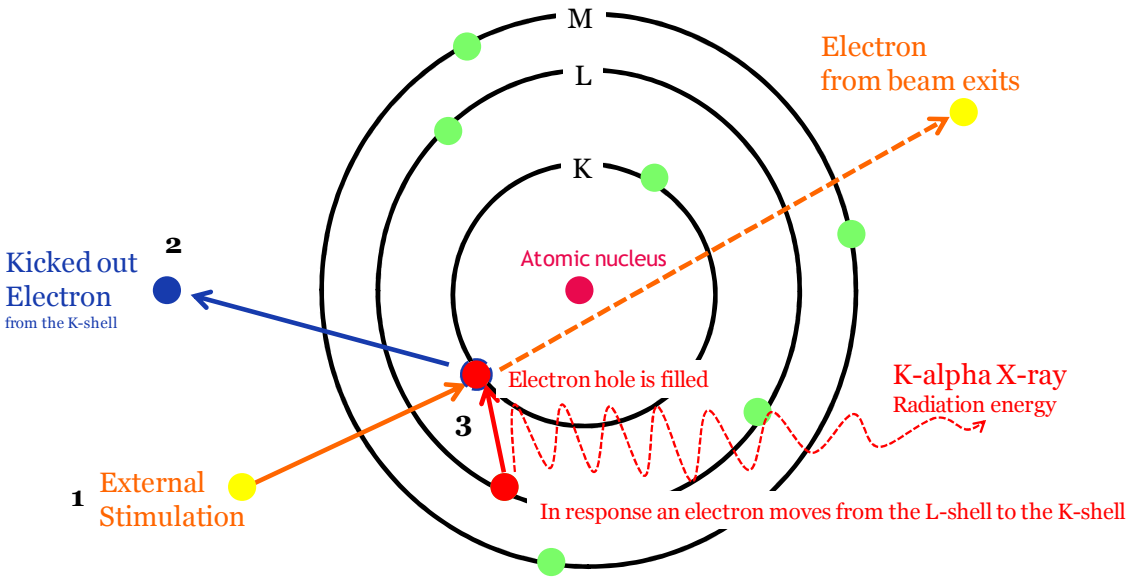

Figure 13: EDS process model

The particle samples were mounted onto an SEM sample peg using double sided tape and then sputter coated with palladium and gold in order to make the samples

conductive. Operating conditions for EDS were set to be at a range of electron beam accelerating voltages from 15 kV to 25 kV with a magnification of 430 at a take-off angle of 40 °. The spectra resolution was 100 eV.

6-2-2-4-2. Wavelength Dispersive X-ray Spectroscopy

Wavelength dispersive x-ray spectroscopy (WDS) measures the wavelengths of the x-rays and was conducted using a JEOL JXA-8900R WD/ED Combined Microanalyzer instrument. Results show an x-axis of the l-number (mm) which represents the distance between the crystal and the sample in the spectrometer as it diffracts the x-rays. The operating conditions for performing the WDS scan were set at an accelerating voltage of 25 kV, a magnification of 430, and covered the range of 175 mm to 168 mm in order to decipher the molybdenum peak from the sulfur peak.

6 -2-3. Fabrication of High Surface Area Nanogrooved Electrospun Fibrous Membranes

6-2-3-1. Preparing the Electrospinning solution:

A 5-mL 15% w/v polymer solution was prepared by weighing 0.45 g of cellulose acetate (CA) and adding this to a weighed amount (0.3 g) of polyethylene oxide (PEO). This 60/40 CA:PEO mixture of solids was then added to a vial and a 60/40 volume ratio of acetonitrile to acetone was added to make a 5-mL solution. A small stir bar was immediately put into the vial, and the vial was sonicated for 30 min and then stirred at room temperature on a high speed for 1 h. The solution was then used immediately after this agitation in order to ensure that the polymers remained evenly dispersed throughout the one hour electrospinning process that took place at room temperature. Tables 1 and 2

provide information on the physical properties and solubility of the polymers and solvents used for co-continuous electrospinning.

Table 1: Properties of Solvents

Solvent	**Acetonitrile**	**Acetone (Ac)**
Molar mass (g/mol)	41.1	58.1
Boiling point (°C)	81.6	56.2
Vapor Pressure (mmHg, 20°C)	73	184
Surface tension (dyn/cm, 20°C)	29.3	23.7
Viscosity(cP, 25 °C)	0.343	0.308
Solubility parameter[a] (δ, MPa)$^{1/2}$		
δ_{total}	24.3	19.9
$\delta_P/\delta_D/\delta_H$	18.0 / 15.4 / 6.1	10.4 / 15.5 / 7.0

a. δ_P: polar interaction, δ_D: dispersion force, δ_H: hydrogen bond

Table 2: Polymer Properties

Polymer	Cellulose acetate (CA)	Polyethylene oxide (PEO)
Molecular weight (g/mol)	30,000 (M_n)	87,000 (M_n)
Transition temperature (°C)	67 (T_g)	65 (T_m)
Solubility parameter[a] (δ, MPa)$^{1/2}$		
δ_{total}	25.1	20
$\delta_P/\delta_D/\delta_H$	12.7 /18.6 / 11.0	3.0 / 17.3 / 9.4

T_g: glass transition temperature, T_m: melting temperature

6-2-3-2. Electrospinning

After solution preparation, the solution was immediately loaded into a 5-mL plastic syringe for electrospinning. A syringe pump (PHD Ultra Pump; Harvard Apparatus, Holliston, MA) infused the polymer solution at speed of 0.05-mL/min through a stainless steel needle (Hamilton, Reno, NV) with a diameter of 0.016 in (0.41 mm) (Hamilton N722 and N720, Reno, NV). A 15-kV voltage was applied between the needle and an aluminum

foiled wrapped Teflon® collection plate (12 in^2 surface) that was 15 cm from the syringe needle tip. An electric field was generated by the voltage between the needle tip and the collection surface enabling electrospun fibers to be deposited on the plate forming a nonwoven nanofibrous mat. Experiments were conducted at room temperature. Electrospinning was conducted for 1 h in order to fabricate a dimensionally stable and thick fibrous membrane that could be easily pealed off of the foil using tweezers after vacuum drying. The foil collection plate with the nanofibrous web composed of 60% cellulose acetate and 40% polyethylene oxide was then removed from the Teflon® plate, placed in the vacuum oven and vacuum dried for a minimum of 8 h at room temperature. Figure 14 illustrates the electrospinning set-up used to fabricate the membranes.

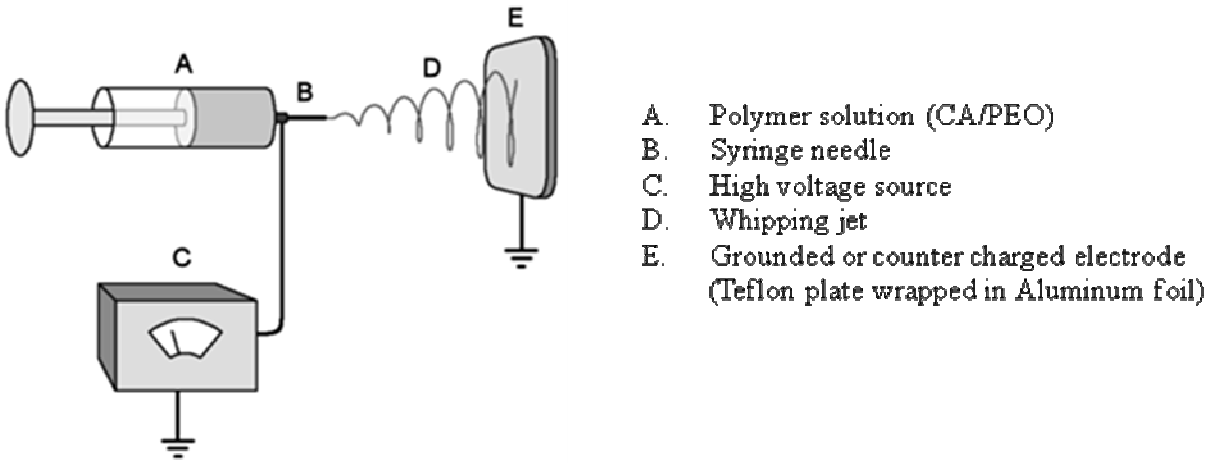

Figure 14: Electrospinning cellulose acetate / polyethylene oxide membranes

6-2-3-3. Soxhlet Extraction

After being vacuum dried, the nanofibrous electrospun fiber mats were carefully peeled from the foil using tweezers. They were then cut in half, ensuring that both halves were the same weight, and one half was reserved and stored under vacuum until future experiments, where it was referred to as a "non-extracted / non-grooved" fibrous

membrane. The second half was rolled gently into a loose roll using tweezers and placed in a thimble filter. The thimble filter was then placed in the glassware depository to conduct a Soxhlet extraction at 80 °C using HPLC grade deionized water for 22 h to remove the PEO component of the portion from the 60/40 CA/PEO fiber mat. The Soxhlet extraction apparatus shown in Figure 15 was chosen to avoid causing structural damage to the fiber mat and to enable continuous, distilled, hot water circulation over the long duration of extraction that was necessary to remove the PEO. The extracted fibrous membranes were then removed from the thimble filter with tweezers and vacuumed dried at room temperature for a minimum of 8 h.

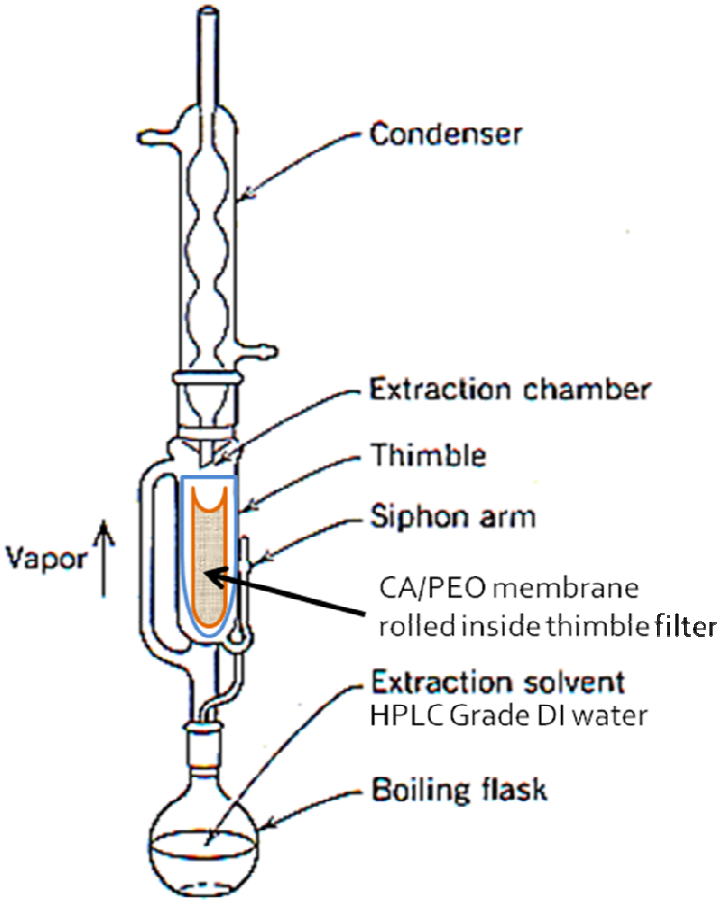

Figure 15: Soxhlet extraction of nanofibrous membrane

6-2-4. Characterization of High Surface Area Nanogrooved Electrospun Fibrous Membranes

6-2-4-1.Fourier-Transform Infrared Spectroscopy (See 6-2-2-1)

The explanation for the FTIR theory and technique can be found in section 6-2-2-1. Membrane samples were measured using a Nicolet Magna-IR 560 spectrometer. For the electrospun membranes, the FTIR spectrum was used to indicate the addition or loss of material, functional groups, or whole compounds such as the loss of polyethylene oxide, which was expected after the membrane underwent a Soxhlet extraction. FTIR spectrums for cellulose acetate and polyethylene oxide polymers were measured separately from each other in powder form and compared to results found in the literature. Figure16 (a) shows a peak at 2891cm^{-1} as characteristic of the molecular absorption of pure polyethylene oxide (Ramesh et al., 2008). Figure 17 shows the FTIR spectrum for a cellulose acetate membrane with characteristic peaks around 1032 cm^{-1}, 1225 cm^{-1}, and 1747 cm^{-1} (Dixit et al., 2010).

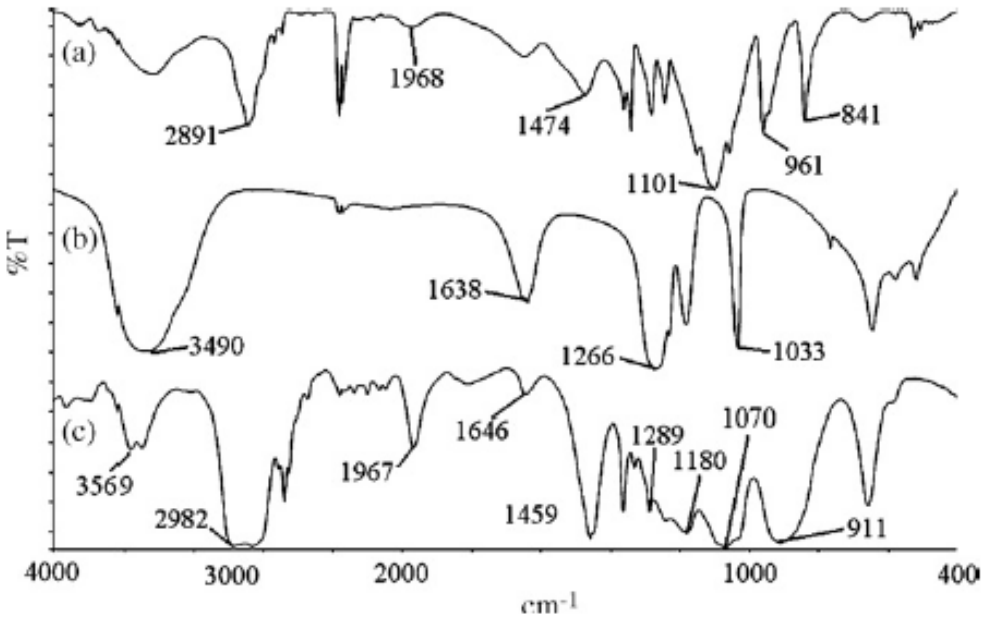

Figure 16: (a) FTIR of pure polyethylene oxide (Ramesh et al., 2008)

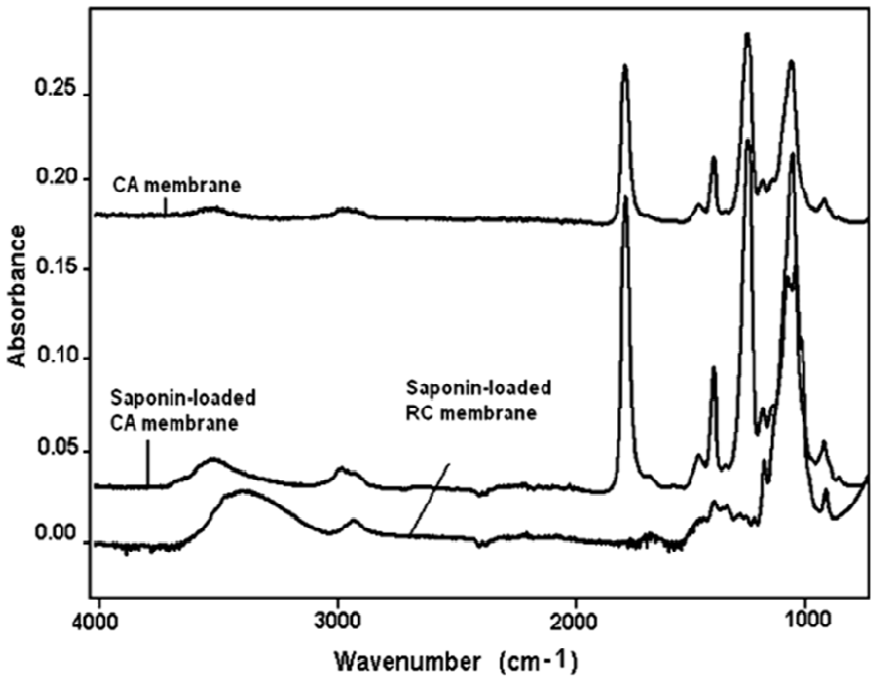

Figure 17: FTIR of a cellulose acetate electrospun membrane (Dixit et al., 2010)

6-2-4-2. Scanning Electron Microscopy (See 6-2-2-3)

Section 6-2-2-3 describes the theory and procedures for this technique. Scanning electron microscopy (SEM) on a Leica 440 (Leica Microsystems, Wetzlar, Germany) was used to analyze the membranes. The membrane samples were sputter coated with palladium and gold in order to make the samples conductive. As mentioned previously, higher voltage results in a higher resolution image. Therefore, the clearest images of the membrane fibers were captured using the low voltage of 5 keV

6-2-4-3. Capillary Flow Porometry

The pore size distribution and average pore diameter of the membranes were measured using a Porous Materials, Inc (PMI) Capillary Flow Porometer CFP-1100-AEHXL (Ithaca, NY). The samples were mounted in the test chamber and the following test parameters were used: Dry up / Wet up, diameter = 20 mm, Silwick®, and 20.1 dynes / cm. First the porosity of the membrane was characterized dry. Then the membrane was wetted with Silwick®, and its porosity was characterized. The mean flow pore diameter and pore size distribution of non-extracted / non-grooved membranes were compared to those of the extracted / grooved membranes.

6-2-4-4. Molecular Gas Adsorption: BET Surface Area Measurement

The surface areas of the cotton swatches and the membranes were determined using the Brunauer, Emet, Teller method known as BET. In the case of the BET technique used for the cotton swatches, the surface area of the fabric was measured via nitrogen adsorption at -195°C on Micrometrics BET Sorptometer. In the case of the BET technique used for the membranes, the surface area of the fabric was measured via krypton adsorption at -195°C on a BET Sorptometer at Porous Materials, Inc by their analytical services in Ithaca, NY. The krypton gas adsorption method was chosen to accommodate low surface area analysis. Measurement of very low surface areas by nitrogen adsorption can lead to less accurate measurements due to the high detection limits posed by the equipment. At surface areas lower than $1m^2$ the number of nitrogen molecules desorbed in the void volume of the test cell can exceed the number of molecules actually adsorbed by the sample surface. This will contribute to greater instrument uncertainty. This uncertainty can be decreased by increasing the sample size tested.

Krypton adsorption is the recommended alternative to overcome this challenge of obtaining accurate measurements since it improves the detection limit significantly and can measure surface areas as low as 0.05 m^2 or less. This is due to lower vapor pressure of krypton. Its low vapor pressure causes less molecules to accumulate in the void volume of the test cell thus avoiding inaccuracies. At 77.4 K krypton is about 38.5 K below its triple point temperature (Tr = 115.35K). It sublimates (i.e., P_0, solid) at a pressure of approximately 1.6 torr. The saturation pressure of supercooled liquid krypton is 2.63 torr. When plugged into the BET equation, this means that the number of molecules in the free space of the sample cell is significantly reduced to approximately 1/300 that of the nitrogen case making krypton the more accurate choice for surface areas less than 1 m^2, particularly surface areas as low as 0.05 m^2 or below (Quantachrome, 2012).

The surface area of the fibers available to the krypton vapor for the non-extracted / non-grooved membranes was compared to that of the extracted / grooved fibers to see if an increase in surface area had been achieved by extracting PEO from the co-continuous structure. These surface areas were then compared to the surface area of cotton as measured by nitrogen gas adsorption.

6-2-5. Grafting $H_5PV_2Mo_{10}O_{40}$ to the Non-grooved and Grooved Electrospun Fibrous Membrane

After the specimens had been vacuumed dried, they were weighed on the analytical balance (accuracy to 1 mg), and a 100 mL grafting bath of 5% v/v hexamethyl diisocyanate (HMDI) and 0.25% v/v tin II catalyst was prepared and poured into a glass three-neck, 200- mL reaction flask. The specimen and a small stir bar were immediately placed into

the flask using tweezers. This flask had initially been vacuum purged, and once it was filled with the HMDI solution, the flask was held under nitrogen purge for the remainder of all grafting reactions due to the moisture sensitivity of the diisocyanate. The temperature of the grafting bath was raised to 70°C while the bath and specimen were stirred for 1 h. After being functionalized with HMDI for 1 h, the specimen was removed from the flask and placed in a toluene bath for 4 h at room temperature (RT), a second toluene bath for 4 h at RT, and then a third toluene bath for 4 h at RT. These subsequent toluene baths were used to remove any unreacted HMDI from the functionalized substrates. The specimen was then vacuum dried overnight at RT, and characterized using FTIR.

After characterization to confirm the HMDI surface functionalization, the specimen were placed in a 200 mL three neck flask that contained a 20% w/v grafting bath of $H_5PV_2Mo_{10}O_{40}$ POM in toluene held under nitrogen purge at a temperature of 45°C. A stir bar was used to agitate the specimen in the solution for 24 h. After grafting for 24 h, the specimen was removed and placed in a toluene bath for 4 h at RT, a second toluene bath for 4 h at RT, and then a third toluene bath for 4 h at RT. These subsequent toluene baths were used to remove any unreacted POM from the grafted substrates. The specimen was then vacuum dried overnight at RT. After being dried, the specimen was weighed and characterized using FTIR. The functionalization and grafting process of the specimen can be seen in Scheme 5.

Scheme 5: Grafting of cellulose with diisocyanate/tin (II) catalyst in toluene (1) then grafting POM to functionalized surface of cellulose (2)

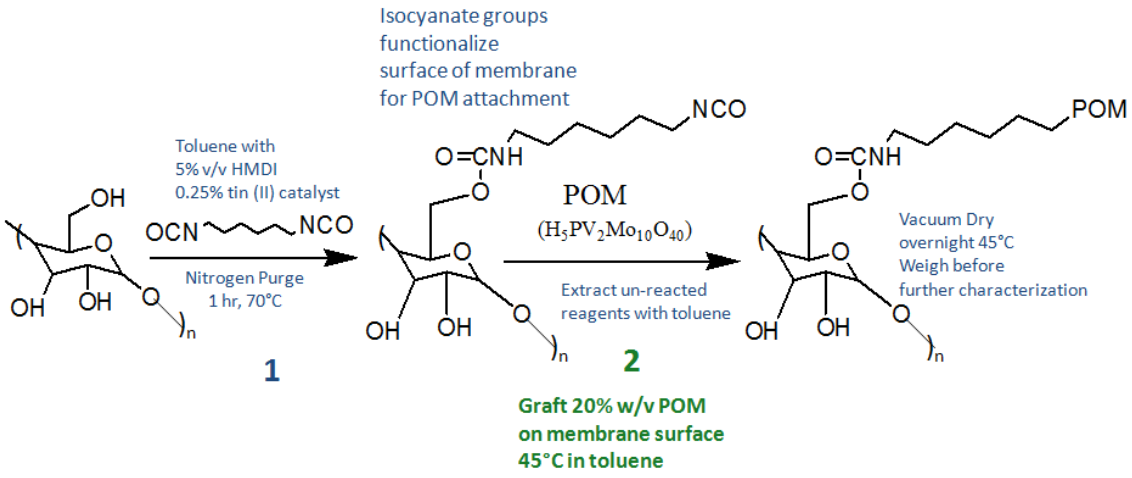

6-2-6. Characterization of $H_5PV_2Mo_{10}O_{40}$ Grafted Membranes

6-2-6-1. Fourier Transform Infrared Spectroscopy (see 6-2-2-1)

The explanation for the FTIR theory and technique can be found in section 6-2-2-1. Grafted membrane and cotton fabric specimen were measured using a Nicolet Magna-IR 560 spectrometer. The FTIR spectrum was used to indicate the functionalization of the membrane or cotton fabric with HMDI and then was used to determine if the POM had been grafted onto the HMDI functionalized substrate surface. FTIR spectrums for HMDI (in liquid form) and $H_5PV_2Mo_{10}O_{40}$ POM (powder form) were used as controls in order to interpret FTIR peaks generated by the functionalized and grafted specimens.

6-2-6-2. Thermogravimetric Analysis

Thermogravimetric analysis (TGA) was used to help characterize the thermal properties of the POM grafted substrates. The three most important parameters in this test are the initial mass of the POM grafted substrate, the temperature of decomposition of the polymer components, and the overall temperature changes in each decomposition step. In TGA, the sample is heated to a high enough temperature so that one of the components decomposes into gas. The decomposition temperature and known chemical formula and stoichiometry of the POM and membrane or swatch may be used to determine the percent add-on of POM by mass ratio (Mansfield, 2010). If the compounds in the POM grafted substrate that remain after being heated (namely the metals molybdenum and vanadium) are known, then it may be possible to determine the percentage add-on of POM on the POM grafted substrate. The weight loss curve may require extensive interpretation in order to understand which components have decomposed at which temperatures. Figure 18 provides general TGA decomposition information for materials (Herguth, 2002).

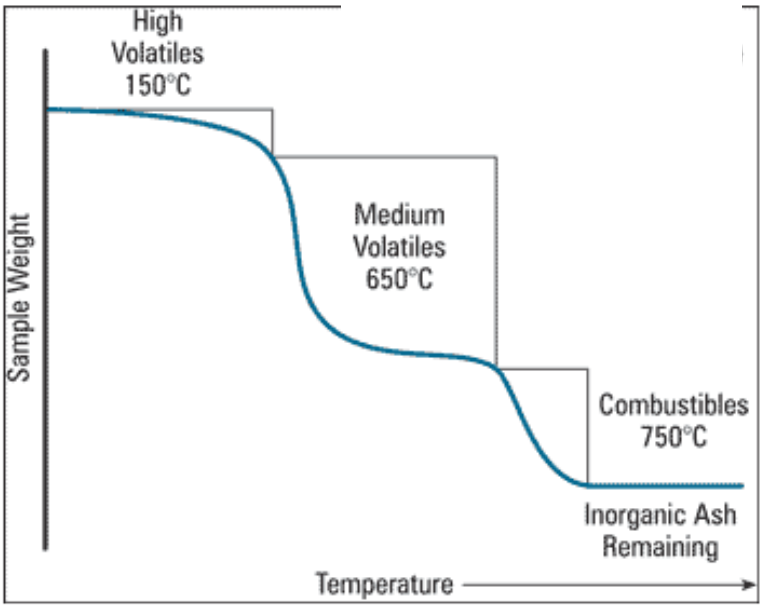

Figure 18: TGA general profile of volatiles (Herguth, 2002)

6-2-7. Decontamination of Methyl Parathion by POM/Cellulose Membrane

6-2-7-1. High Performance Liquid Chromatography

A method was developed using HPLC-DAD (High Performance Liquid Chromatography / diode-array UV/VIS detector) by Lange et al., 2012 to determine the amount of methyl parathion degradation by metal oxides. This same procedure was used to determine the amount of methyl parathion degradation by polyoxometalates. All compounds were measured with a reverse-phase HPLC combined with a diode array UV-vis detector from the Agilent (Santa Clara, CA) HP series 1200. The injection volume was 20 µL. The set-up is run with an Agilent XDB-C18 reversed phase column with 5-µm particle size and 4.6x150 mm dimension and 25 °C. The mobile phase consists of 50% acetonitrile and 50% water with 0.5% formic acid and ran for 15 min. The UV-vis detector was set to scan at 280 and 320 nm. Retention time of methyl parathion was noted, and it was ensured that its peak was separated sufficiently.

A calibration curve relating the concentrations of methyl parathion to the peak area given by the HPLC-DAD was replicated from Lange's procedure by making a 100 mg/L stock standard solution of methyl parathion in hexane. Methyl parathion was dissolved in hexane at the following concentrations: 0.25, 0.5, 5, 10, 25 mg/L, and it was determined that equation 2 represents the relationship between methyl parathion concentration and the HPLC-DAD. The result of this equation was then multiplied by volume to obtain the mass of methyl parathion. Wavelength scans were set for 230 nm, 280 nm, and 320 nm. The 320 nm wavelength was used to detect the maximum amount of methyl parathion. The concentration of methyl parathion was converted to mass amounts by knowing the amount of methyl parathion in the known volume of hexane solution and

using this information to determine the mass amount of methyl parathion present for testing.

$$Peak\ Area\ (mAU) = 69.677 * Methyl\ Parathion\ Concentration\ (^{mg}/_{L}) \quad [2]$$

6-2-7-2. Examining Degradation Products and Retention Times

Standards for the expected degradation products of p-nitrophenol and methyl paroxon were analyzed using the HPLC-DAD to determine their retention times. The standard solution for p-nitrophenol was made at a concentration of 0.070 g/L in HPLC grade deionized water, and the standard solution for methyl paraoxon was made at a concentration of 0.4 g/L in hexane. These solutions were sonicated for 30 min prior to testing. After achieving complete dissolution, 1.5 mL of these solutions were taken with a syringe. A syringe filter was attached, and the filtered solutions were transferred to the corresponding HPLC vial. These samples were analyzed on the HPLC-DAD using the method described in section 6-2-7-1. Each time the degradation performance of the polyoxometalate loaded substrates was measured, these standard solutions of degradation products were made and analyzed on the HPLC-DAD so that degradation products resulting from the POM decontamination could be easily recognized by the retention times of the peaks.

6-2-7-3. Reaction with Methyl Parathion and POM

6-2-7-3-1. Reaction of Methyl Parathion and POM in Powder Form

A standard solution of 0.016 g /L methyl parathion in hexane was made and sonicated for 30 min. To ascertain the decontamination performance of the polyoxometalates in powder form before being grafted onto the fabric, three solutions of

POM powder in a methyl parathion / hexane were made at 5%, 10%, and 20%. These solutions were agitated on a roller mixer for 1 h, left to set for 24 h, and then 1.5 mL of each of the three solutions was filtered and transferred to HPLC vials. These solutions were then analyzed on the HPLC-DAD using the method detailed in 6-2-7-1. A standard solution of 0.016 g/L methyl parathion and the degradation product standard solutions were analyzed as well using the method detailed in 6-2-7-2.

6-2-7-3-2. Reaction of Methyl Parathion and POM Grafted Cotton

A standard solution of 0.016 g /L methyl parathion in hexane was made and sonicated for 30 min. To determine the decontamination performance of the polyoxometalates grafted, the cotton specimen was vacuumed dried for 8 h and then placed in a sealed container of 200 mL of the methyl parathion standard solution. Four aliquots were withdrawn by a syringe, filtered, and placed in 1.5 mL HPLC vials at the initial time, after 2, 10, and 24 h. The cotton specimen was then removed from the container, vacuum dried, and stored in a vacuum desicator. These solutions were then analyzed on the HPLC-DAD using the method detailed in 6-2-7-1. A standard solution of 0.016 g/L methyl parathion and the degradation product standard solutions were analyzed as well using the method detailed in 6-2-7-2.

6-2-7-3-3. Reaction of Methyl Parathion and POM Grafted Membranes

A standard solution of 0.016 g /L methyl parathion in hexane was made and sonicated for 30 min. To determine the decontamination performance of the polyoxometalates grafted onto the non-grooved fiber membranes and the grooved fiber

membranes, the membrane (whether grooved or non-grooved) was vacuumed dried for 8 h at RT and then placed in a sealed container of 200 mL of the methyl parathion standard solution. Aliquots were withdrawn by a syringe, filtered, and placed in 1.5-mL HPLC vials at varying time intervals between 20 min and 24 h. The membrane was then removed from the container, vacuum dried, and stored in a vacuum desicator. These solutions were then analyzed on the HPLC-DAD using the method detailed in 6-2-7-1. A standard solution of 0.016 g/L methyl parathion and the degradation product standard solutions were analyzed as well using the method detailed in 6-2-7-2.

6-2-8. Statistical Analysis

Each treatment (non-grooved fibers, grooved fibers, and cotton) had 3 replicate samples tested for methyl parathion degradation. Repeated measures ANOVA tests were completed to analyze if the mean amount of methyl parathion degradation was significantly different between treatments. This particular type of ANOVA was chosen to account for the fact that all samples of the random data set were measured under a number of different time conditions. As each sample was exposed to each new time condition, the measurement of the dependent variable (amount of methyl parathion degradation) was repeated. Using a standard ANOVA in this case is not appropriate because the data violate the ANOVA assumption of independence. A traditional ANOVA model also would fail to model the correlation between the repeated measures.

6. Results and Discussion

7-1. Characterization of Polyoxometalate $H_5PV_2Mo_{10}O_{40}$ Synthesis:

7-1-1. Fourier-Transform Infrared Spectroscopy

When considering what functional groups to analyze and identify from the FTIR spectrum of the POM, it is important to consider the structure and geometry of $H_5PV_2Mo_{10}O_{40}$. The heteropoly anion consists of a central phosphate (PO_4^-) tetrahedron encompassed by ten molybdenum oxide (MoO_6) octrahedra (square bipyramid of MoO_3), and two vanadium oxide (VO_5) trigonal bipyramids (Pope, 1983). As a mixed addenda Keggin unit with some reduced structural symmetry (due to the incorporation of vanadium in addition to the phosphorus and molybdenum heteropolyanions), the chemical structure of this POM can be correlated with five to six characteristic peaks or bands found in the IR spectrum of the experimental POM synthesis product (Pope, 1983; Moffat, 2001; Arichi et al., 2010). Expected functional groups to examine include P-O, Mo-O, and V-O, singly or doubly bonded with differing bond lengths and angles (Nakamoto, 1986; Misono and Okahura, 1993; Popa et al., 2006; Arichi et al., 2008; Arichi et al., 2010). The bond geometry, stretching, and vibrational modes of the functional groups determine the location of their absorption bands on the spectrum (Nakamoto, 1986; Gratton et al., 1978; Moffat, 2001). For example, the inter-octahedral M-O-M (M: Mo or V) vibrations can occur at the same and/or different wavenumbers than the intra-octahedral M-O-M vibrations depending on the size of the bond angles. Further examination of the IR spectroscopy literature provided correlating band values for compounds such as PO_4^{3-} (phosphate anion), MoO_3 (molybdenum trioxide), V_2O_5 (vanadium pentoxide), HSO_4^- (hydrogen sulfate), Na_2MoO_4 (sodium molybdate), and closely related molybdate,

vanadate, and molybdovanadate POM structures (Nyquist and Kagel, 1971; Nakamoto, 1986; Almond et al., 1989; Ramirez et al., 1990; Robinson, 1991; Hug,1997; Moffat, 2001; Selim and Sparks, 2001; Popa et al., 2006).

Figure 19 (a) shows the FTIR spectrum of the synthesized particles with absorption bands at 3462, 1650, 1160, 1060, 856, 775, and 600 cm^{-1}. The strong, broad band at 1160 cm^{-1} correlates well with the central phosphate tetrahedral anion (Nyquist and Kagel, 1971; Robinson, 1991). The strong, broad band at 1060 cm^{-1} correlates closely with the Mo=O, P-O functional groups, and the stretching mode of V=O, as well as peaks seen in the literature for PO_4^{3-}, MoO_3, and V_2O_5 (Nyquist and Kagel, 1971; Robinson, 1991; Misono and Okahura, 1993; Kozhevnikov, 1998; Zidan et al. 2000; Arichi et al., 2008; Arichi et al., 2010). A strong, broad peak at 856 cm^{-1} correlates closely with MoO_3 and V_2O_5 compound spectras and also can be attributed to the M-O-M vibrations of a doubly bridging oxygen connecting two contiguous chains in the structure. This broad peak encompasses part of the region (722-840 cm^{-1}) where these M-O-M vibrations occur when the bond angles of the complexes are greater than 140° (Nyquist and Kagel, 1971; Gratton, et al., 1978; Robinson, 1991; Popa et al., 2006).

The observed IR peaks of the experimentally synthesized POM correspond well with what has been seen in the literature (Misono and Okahura, 1993; Kozhevnikov, 1998; Popa et al., 2006; Arichi et al., 2008; Arichi et al., 2010) for this POM as seen in Figure 19 (b). Arichi et al., 2008 & 2010, found peaks at 3422, 1618, 1160, 1060, 958, 866, 784, and 590 cm^{-1}. By comparing my spectrum in Figure 19 (a) to that of the literature in Figure 19 (b), it is evident that some differences exist, particularly in terms of the peak intensity, but that a structure very similar to $H_5PV_2Mo_{10}O_{40}$ was the result of my synthesis. The strong

peak intensity at 1060 cm^{-1} in the spectrum of the synthesized POM (%T = 97.37) was compared to the peak intensity of the 1060 cm^{-1} peak found in Arichi et al., 2010 (%T ~ 50). The resulting peak ratio showed that Arichi's POM compound possessed almost twice the intensity of the experimentally synthesized compound. Earlier spectrums (not shown herein) of the experimentally synthesized POM exhibited a much greater peak intensity at 1060 cm-1 (%T = 36.06) which would have improved the peak intensity comparison significantly; however, the intensity at all peaks changed as the synthesized particles aged in a vacuum desicator over the course of time it took to conduct experiments. Other differences between earlier spectrums of the experimentally synthesized POM particles revealed more defined broad peaks at 1647 cm^{-1} (%T = 86.74) and at 3398 cm^{-1} (%T = 81.99) which corresponded well to the peaks at 1618 cm^{-1} (%T~58) and 3422 cm^{-1} (%T~47) found in Arichi et al., 2010. Broad bands seen in these regions of the spectrum (3300-3400 cm^{-1}, 2240 cm^{-1}, and 1610-1650 cm^{-1}) are correlated with the presence of water in the sphere coordination (secondary structure) and reflect the stretching [asymmetric, symmetric, and bending] fundamentals of residual lattice moisture (Almond et al., 1989; Moffat, 2001; Arichi et al., 2010). Because the particles were stored in a vacuum desicator over the course of testing to help remove residual water, the bands in this region of the spectrum seen in Figure 19 (a) have a lower intensities than the bands seen in the residual water region of the literature POM spectrum in Figure 19 (b). The experimental IR spectrum shown in Figure 19 (a) was measured at the time that the particles were used for the grafting process and, therefore, is the best representation of the chemical identity of the particles at the time of the decontamination testing.

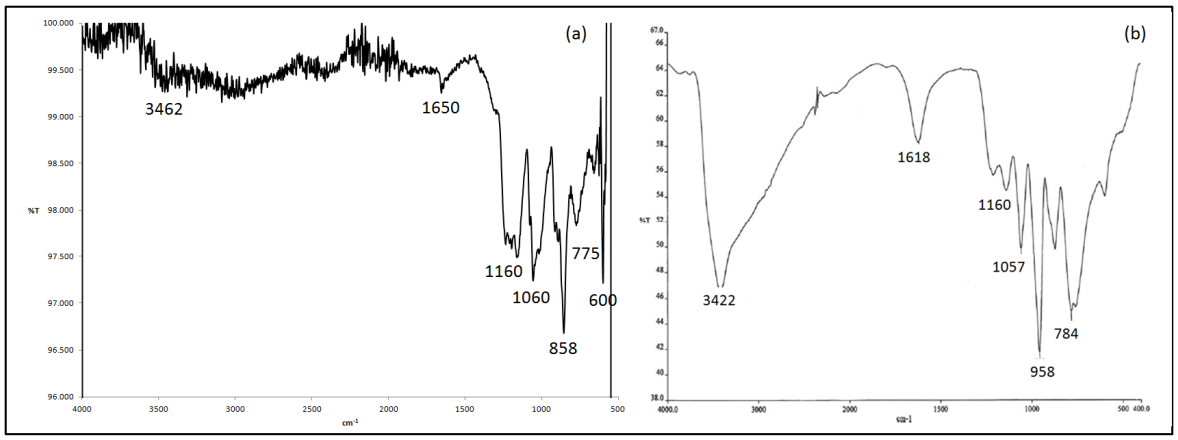

Figure 19: FTIR % Transmittance Spectrum of $H_5PV_2Mo_{10}O_{40}$ (a) from experimental synthesis & (b) spectrum from literature (Arichi et al., 2010)

Table 3 identifies the key IR bands of Figure 19 (a) & (b) and their spectral interpretation (Nyquist and Kagel, 1971; Gratton et al., 1978; Pope, 1983; Nakamoto, 1986; Almond et al., 1989; Ramirez et al., 1990; Robinson, 1991; Misono and Okahura, 1993; Hug,1997; Kozhevnikov, 1998; Neumann, 1998; Zidan et al., 2000; Selim and Sparks, 2001; Popa et al., 2006; Arichi et al., 2008; Arichi et al., 2010; Larkin, 2011).

Table 3: Comparison of IR bands of the synthesized $H_5PV_2Mo_{10}O_{40}$ and $H_5PV_2Mo_{10}O_{40}$ of Arichi et al., 2010, and the Spectral Interpretation

Sample	Bands & Key Peaks (cm^{-1}) Range 4000 - 550 cm^{-1}	Peak Height (% Transmittance)	Infrared Correlation Compound
$H_5PV_2Mo_{10}O_{40}$ - Experimental Synthesis	3462	99.27	residual lattice water
	1650	99.36	residual lattice water
	1160	97.51	PO_4^{3-}
	1060	97.55	Mo=O, MoO_3, M-O-M vibrations P-O, PO_4^{3-} V=O, V_2O_5 residual HSO_4^-
	856	96.69	V-O MoO_3, Mo=O residual HSO_4^-
	775	97.83	V-O
	600	97.22	PO_4^{3-} MoO_3 V_2O_5 residual HSO_4^-
$H_5PV_2Mo_{10}O_{40}$ - Arichi et al., 2010	3422	47*	residual lattice water
	1618	58*	residual lattice water
	1160	54*	PO_4^{3-}
	1060	50*	Mo=O, MoO_3, M-O-M vibrations P-O, PO_4^{3-} V=O, V_2O_5
	960	41*	Mo=O, M-O-M vibrations V=O P-O
	866	50*	V-O MoO_3, M-O-M vibrations
	784	45*	V-O
	590	54*	PO_4^{3-} MoO_3

* peak height values were estimated from the %T spectru

Byproducts of the synthesis, which were identified by later analysis with XRD and EDS, may have been one of the causes of the slight deviation of the synthesized compound from the spectral signature and peak intensities found in the literature. The residual hydrogen sulfate present in the POM resulted from using an excess of sulfuric acid in order to achieve the pH of 3.5 for synthesis. Therefore, IR bands for this bi-product can be observed at 1060, 856, and 600 cm^{-1} and may have strengthened the intensity of those peaks (Nyquist and Kagel, 1971; Nakamoto, 1986; Robinson, 1991; Selim and Sparks, 2001; Larkin, 2011). It is also of interest to note that bands in the range of 2200-1200 cm^{-1} are commonly associated with residual impurities that may be contained in the preparative reagents (Moffat, 2001). While weak bands are present in this spectral region of the experimentally synthesized POM, no additional impurities were examined in this study.

7-1-2. X-ray Diffraction (XRD)

The x-ray diffraction peaks for the synthesized $H_5PV_2Mo_{10}O_{40}$ did not correspond to what was seen in the literature as shown in Figure 12 (Arichi et al., 2010). A reflexion at $2\theta = 9°$ is typical for a molybdovanadate Keggin structure (Popa et al., 2006; Arichi et al., 2010). However, most XRD peaks were seen at higher angles between 20°-50° indicating large lattice spacings unlike the XRD peaks found at smaller angles in the literature results. Using the JADE software library matching tool, peak analysis showed the closest matches with the lattice patterns for Na_2SO_4 as seen in Figure20 (a) and $Na_2H(SO_4)_2$ as seen in Figure 20 (b). Matches were also made for crystalline structures of vanadium oxide and molybdenum oxide with the closest matches achieved in the second try at synthesizing $H_5PV_2Mo_{10}O_{40}$. These results do not confirm the presence of

$H_5PV_2Mo_{10}O_{40}$ in its crystalline form. Instead, they indicate that the only crystalline compounds present are Na_2SO_4 and $Na_2H(SO_4)_2$. As a result, further analysis was needed to determine whether $H_5PV_2Mo_{10}O_{40}$ was present and in the amorphous phase.

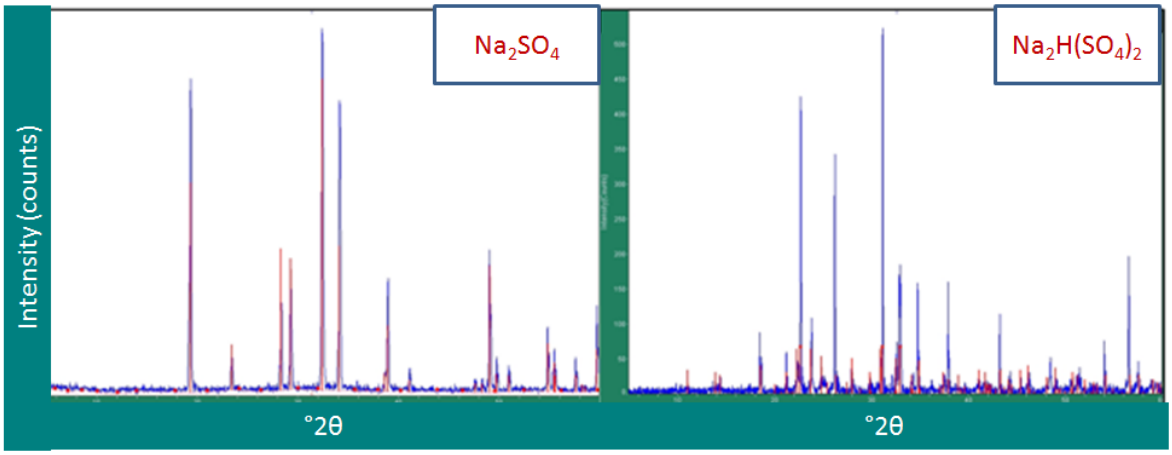

Figure 20: XRD of synthesized particles with Na_2SO_4 synthesis byproduct(a) with $Na_2H(SO_4)_2$ byproduct (b) (Synthesized particles are shown in blue. Byproducts are shown in red.)

7-1-3. Scanning Electron Microscopy

SEM images as seen in Figure 21 and further image J analysis showed the size of the POM particles. Particle size ranged from 500 – 1000 µm which corresponded to the literature (Arichi et al., 2008; Arichi et al., 2010). These particles are larger than the mean pore size of both the non-grooved (9.9 µm) and grooved (6.7 µm) membranes.

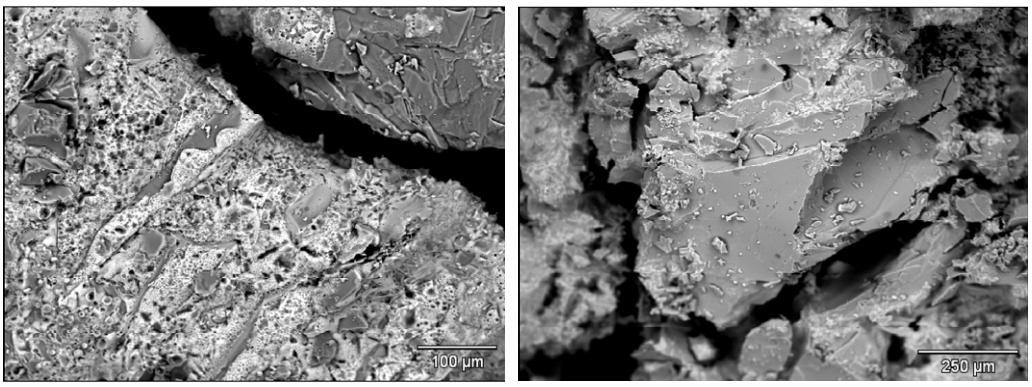

Figure 21: SEM Morphology of synthesized $H_5PV_2Mo_{10}O_{40}$

7-1-4. X-ray Microanalysis

7-1-4-2. Energy Dispersive X-ray Spectroscopy

Energy-dispersive x-ray spectroscopy (EDS) was used to measure the energy of the x-rays and perform elemental analysis of the POM particles. The resulting Figure 22 illustrates the elemental structure of the POM including peaks for the phosphorus, vanadium, molybdenum, and oxygen. Peaks for the Pd and Au sputter coating of the sample, which was necessary to make the sample conductive in preparation for this technique, are also present. The sodium sulfate and hydrogen sodium sulfate byproducts of synthesis that were represented in the XRD pattern mentioned in section 5-1-2 are also apparent. The peak height of each elemental peak can be used as a qualitative representation of the amount of that element present in the structure. WDS was performed to measure the wavelengths of the energy and determine whether the strong EDS peak between 2 and 3 KeV could be attributed to sulfur or molybdenum. From this information, it was determined that the elements of the POM were all present in the synthesized particles. Figure 23 used a colorimetric digital indictor on the SEM of the particles to identify where in the particles these elements were present. This analysis showed an even distribution of vanadium and molybdenum in the particles as well as an even distribution of the other elements seen in the graph in Figure 23.

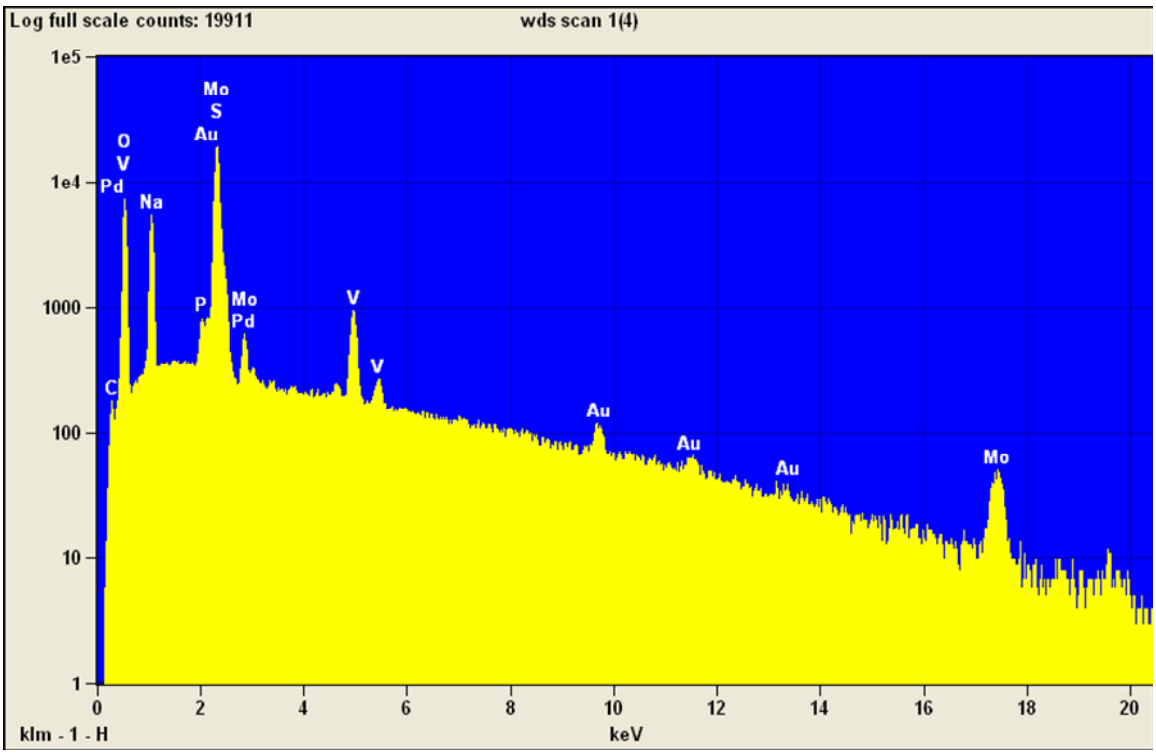

Live Time: 30.0 sec.; Acc.Voltage: 25.0 kV; Take Off Angle: 40.0 deg.

Figure 22: EDS Elemental Analysis of $H_5PV_2Mo_{10}O_{40}$

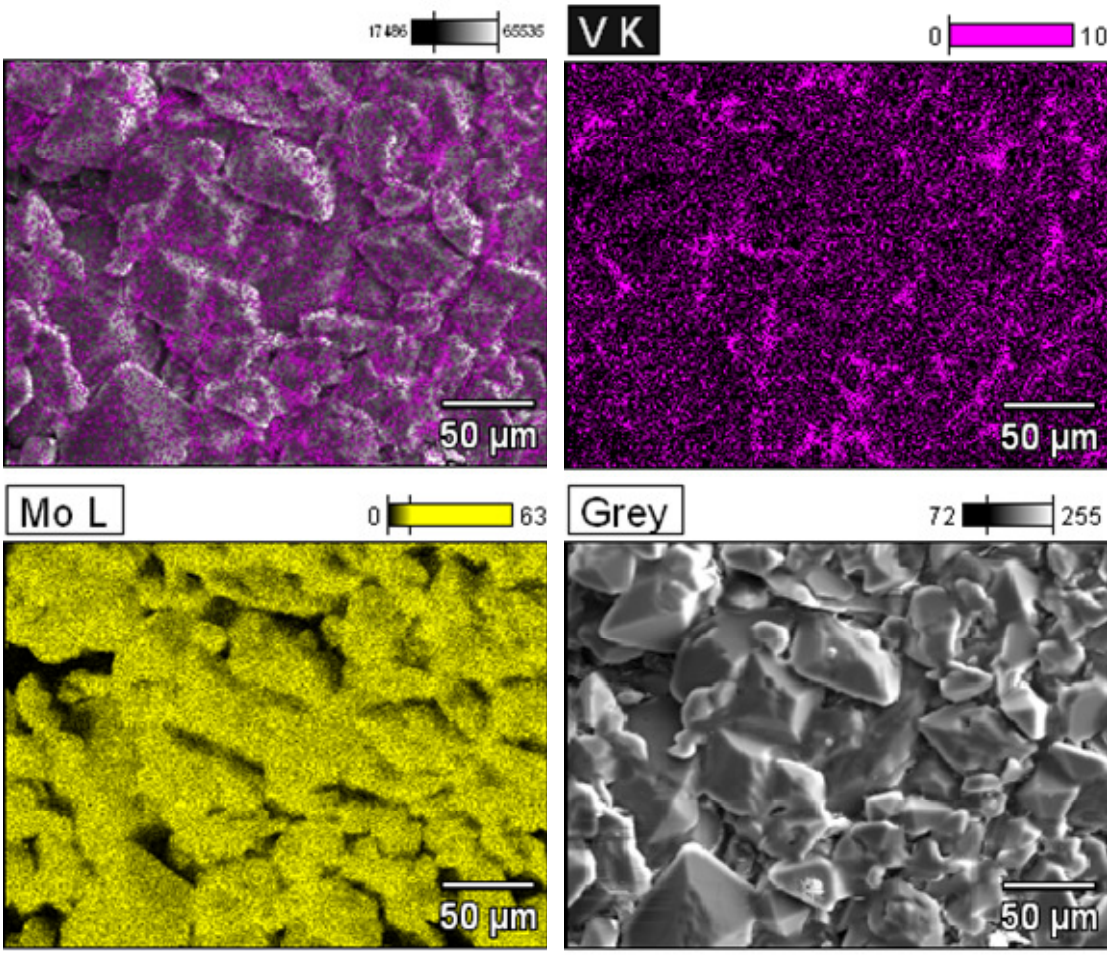

Figure 23: Elemental Analysis using the EDS Scan to confirm the presence of vanadium (V) and molybdenum (Mo) in the $H_5PV_2Mo_{10}O_{40}$ particles (vanadium = magenta, molybdenum = yellow)

EDS confirmed that all elements composing the POM structure were present in the precipitate from the synthesis.

7-1-4-2. Wavelength Dispersive X-ray Spectroscopy

Wavelength dispersive x-ray spectroscopy (WDS) was used to scan the particles in order to determine the specific elemental identity of strong peaks attributed to two elements as seen in the EDS results (Figure 22). In the WDS results, the x-axis is the l-

number (mm) representing the crystal lattice spacing in the spectrometer that is used to diffract the x-rays. Figure 24 shows that the strong peak between 2-3 KeV was due to a greater presence of sulfur than molybdenum. The presence of sulfur can be attributed to the synthesis byproducts of sodium sulfate and hydrogen sodium sulfate.

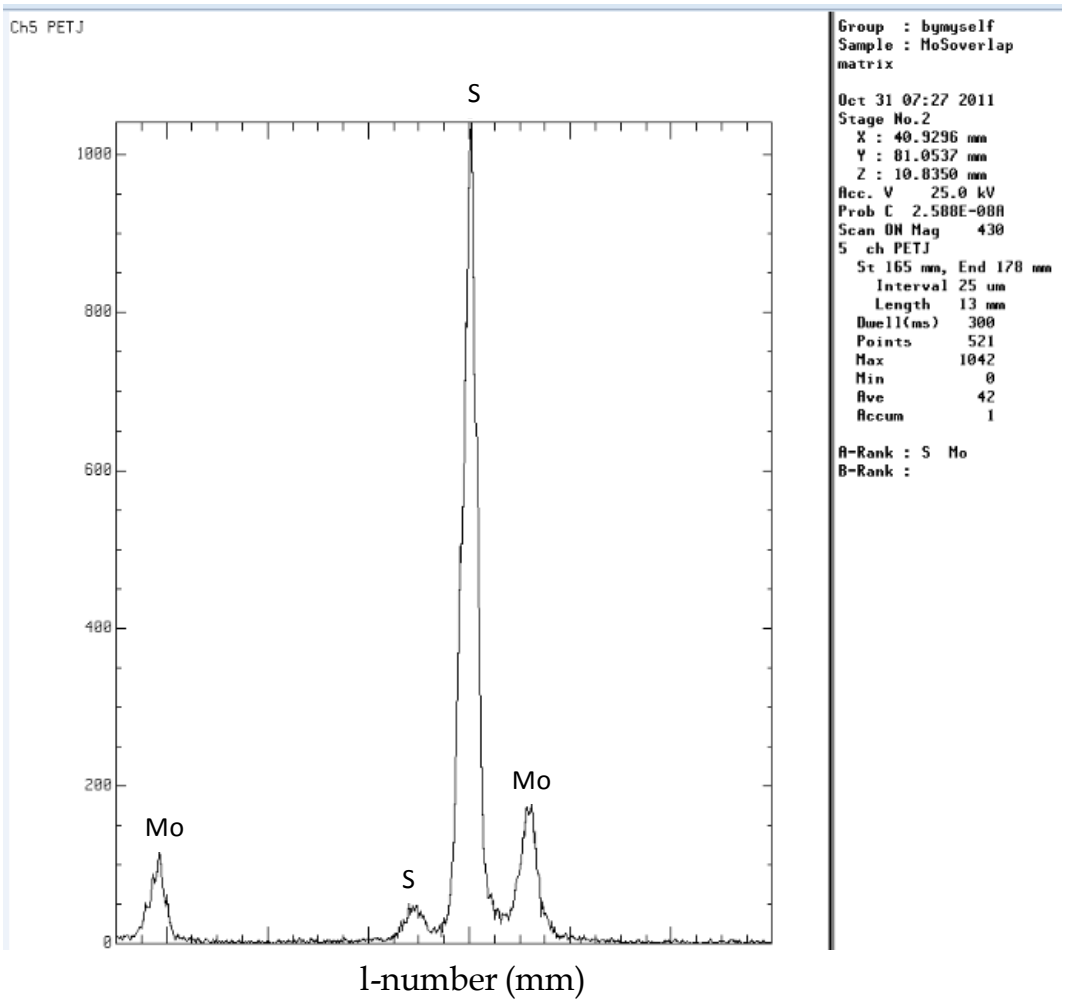

Figure 24: WDS Elemental analysis of the molybdenum and sulfur peak

7 -2. Characterization of High Surface Area Nano-grooved Electrospun Fibrous Membranes

7-2-1.Fourier Transform Infrared Spectroscopy

When the polymers cellulose acetate and polyethylene oxide were analyzed via FTIR spectroscopy in their solid phase, their absorption signature showed major peaks at 1740 and 1032 cm^{-1} for cellulose acetate and at 2879, 1090, and 841 cm^{-1} for the polyethylene oxide. The strong peak at 1747 cm^{-1} correlated with an aliphatic acetate ester functional group, while the strong, broad peak at 1032 cm-1 correlated with the secondary primary alcohol functional groups of cellulose (Robinson, 1991; Larkin, 2011). In examining the changes in the IR spectra after the membranes underwent extraction, the 51% and 48% decrease in the absorption peak heights at 2879 and 1099 cm^{-1}, which were indicative of the aliphatic ether functional groups of polyethylene oxide, can be attributed to the partial removal of PEO in the extraction process. Table 4 summarizes these results for the membranes and offers a spectral interpretation of all key peaks for cellulose acetate and polyethylene oxide. Figure 25 (a) (b) (c) (d) shows the FTIR spectra of the cellulose acetate powder control (a), the polyethylene oxide powder control (b), the non-extracted 60/40 CA:PEO membrane (c), and the extracted 60/40 CA:PEO membrane (d). Figure 25 (a) & (b) spectra were used as standards of comparison when analyzing the electrospun membranes spun from cellulose acetate and polyethylene oxide in a mixed acetone-acetonitrile solvent.

Table 4: Interpreting the FTIR spectra of the electrospun cellulose acetate (CA) / polyethyene oxide (PEO) membranes

Key Peaks (cm^{-1}) Range 4000 - 550 cm^{-1}	Peak Height (Absorbance) 60/40 CA/PEO Non-extracted membrane	Peak Height (Absorbance) 60/40 CA/PEO Extracted membrane	Percent Change in Peak Height (Absorbance)	IR Spectral Interpretation (Robinson, 1991; Larkin, 2011)	
				Correlating Functional Group	Effect on Extracted Membrane
2879	0.035	0.017	-51.43	aliphatic ether (PEO)	removal of PEO
1740	0.081	0.120	48.15	aliphatic acetate ester (CA)	increase in CA peak intensity
1099	0.192	0.099	-48.44	organic ether (PEO)	removal of PEO
1032	0.194	0.237	22.16	secondary primary alcohol (Cellulose)	increase in CA peak intensity
843	0.079	0.031	-60.76	ethyl alkane (PEO)	removal of PEO

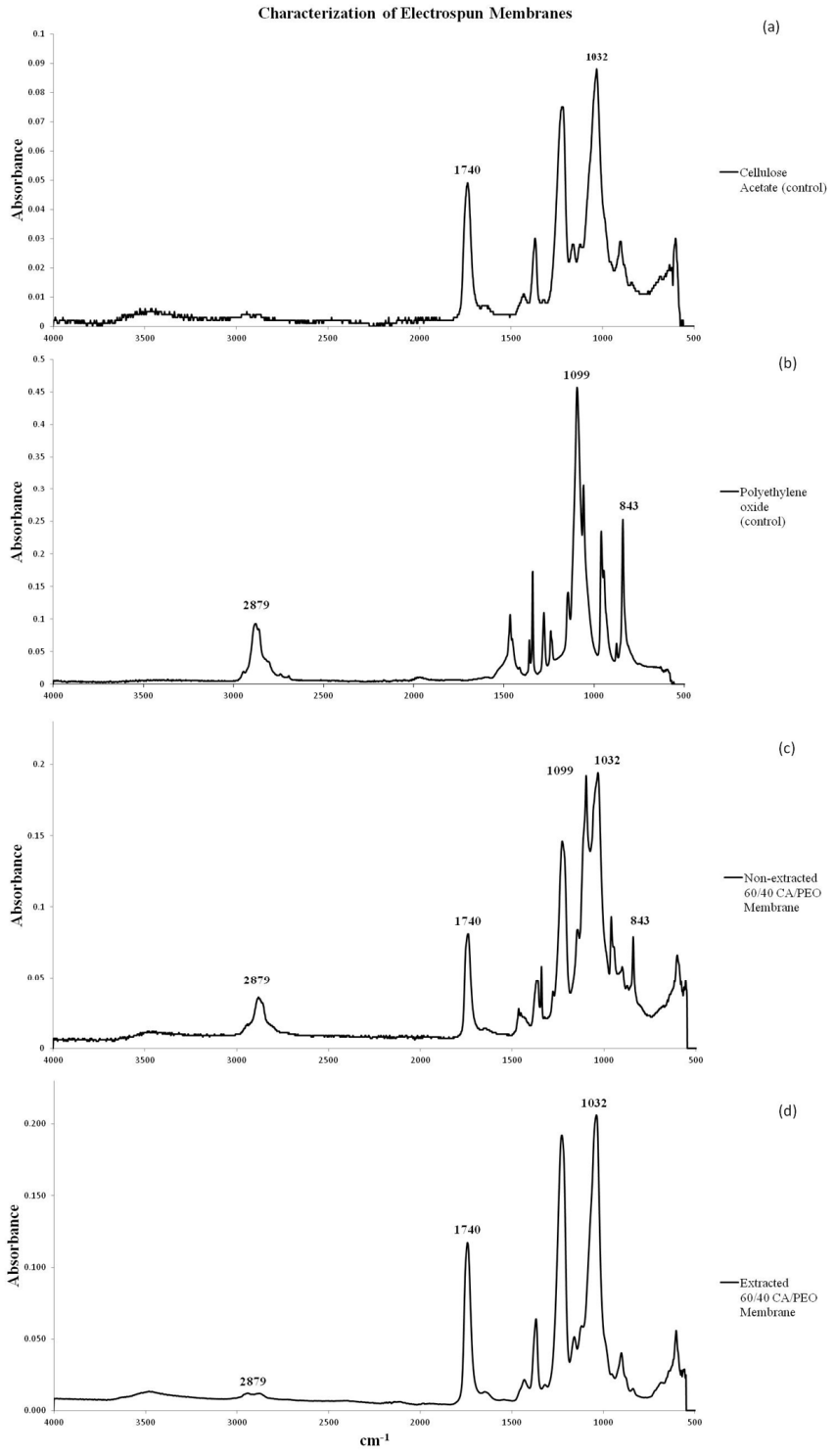

Figure 25: FTIR characterization of cellulose acetate / polyethylene oxide membranes (a) cellulose acetate (control) powder (b) polyethylene oxide (control) powder (c) non-extracted 60/40 CA/40 membrane (d) extracted 60/40 CA/40 membrane [Membranes were made with 60/40 CA/PEO in 60/40 Acn/Ace solvent. Nonextracted membranes are also called "Non-grooved" membranes, while extracted membranes are called "grooved".]

Figure 25 shows the FTIR spectrum of both the (d) grooved/extracted and (c) non-grooved/non-extracted fibers. This spectrum confirms that much of the PEO was removed from the 60/40 CA:PEO membrane via the Soxhlet extraction using boiling deionized water in the grooved fibers as seen by the significant decrease in the size of the peaks at 2879, 1090, and 843 cm^{-1}, which are characteristic of PEO. The presence of small peaks rather than the complete absence of these peaks shows that polyethylene oxide was not completely removed from the membranes; however, initial testing of extracting membranes for a longer amount of time than 22 h resulted in damage to the structural integrity of the membranes as they became stuck to the fibrous thimble filters used in the extraction process. Therefore, testing proceeded with the partially PEO extracted membranes was necessary. The decrease in the size of the other peaks, specifically at 1740 and 1032 cm^{-1}, represent the loss of some cellulose acetate during the extraction process.

7-2-2. Scanning Electron Microscopy

In comparing Figure 26 (a) of the non-grooved / non-extracted fibers to Figure 26 (b) of the grooved / extracted fibers, it is evident that the partial extraction of PEO led to the creation of grooved fiber morphology throughout the structure of the membrane. Figure 26 (a) shows that before extraction, the 60/40 CA:PEO fibers are smooth on their surface, while Figure 26 (b) shows an increase in surface roughness. Achieving this grooved fiber morphology was critical to testing my hypotheses. Image J analysis of SEM figure 26 (a) and (b) of the membranes showed that the fibers ranged from 1 to 2 µm in diameter before and after extraction.

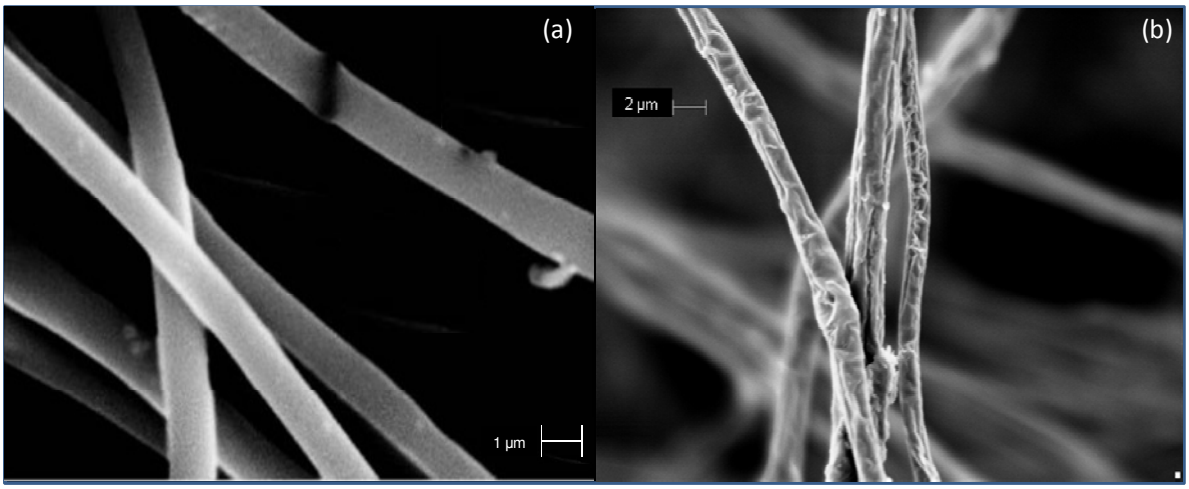

Figure 26: (a) Non-extracted electrospun fibers – 15% w/v 60/40 cellulose acetate / polyethylene oxide (b) Extracted electrospun fibers – 15% w/v 60/40 cellulose acetate / polyethylene oxide fibers with ~ 42% PEO removed after H_2O extraction for 22 h

7-2-3. BET Surface Area Measurement

Table 5 shows the experimental average surface areas achieved by BET gas adsorption on the membranes as well as the cotton swatches. The table also shows the literature values found for cellulose acetate and cotton via nitrogen gas adsorption (Blair and McElroy, 1976; Rowen and Blain, 1947). One-way Anova statistical analysis, as shown in Table 6, of the BET surface area measurements via krypton gas adsorption of the non-grooved and grooved fibrous membranes showed that the increase in surface area between the two treatments was statistically significant with a p-value of 0.0001. A more conservative Wilcoxon / Kruskal-Wallis Test also showed that the increase in surface area for the grooved membranes was statistically significant with a p-value of 0.0197, which is still less than 0.05 and therefore significant. These two data analyses also showed a statistical difference between the surface areas of the membranes and the surface area of the cotton with a p-value of 0.0001. The surface area of 0.63 m^2/g for the grooved 60/40

CA: PEO membranes was higher than the 0.38 m^2/g surface area of cellulose acetate fibers with a traditional CA fiber morphology most likely due the grooved fiber morphology created by the partial PEO extraction. The BET surface area measurements of cotton via nitrogen gas adsorption resulted in an even higher surface area 0.87 m^2/g with a standard deviation of 0.05. This may be due largely to unique morphology of cotton itself that is composed of a network of fine cellulose fibrils and fine surface capillaries. The 0.87 m^2/g surface area of cotton was larger than the 0.72 m^2/g reported in literature; however, it is within expectation of differences in natural fiber and/or BET equipment variations or pertain to the small sample size.

Table 5: BET surface area of membranes and cotton (experimental & literature)

	Area available to krypton molecules at -272.15°C		Area available to nitrogen molecules at -195°C		
Averages	Non-extracted Cellulose Acetate + PEO	Extracted Cellulose Acetate - PEO	100% Unbleached Cotton	Literature (Blair and McElroy, 1976) Cellulose Acetate	Literature (Rowen and Blain, 1947) Cotton
Surface Area (m^2/g)	0.08	0.63	0.87	0.38	0.72
σ	0.02	0.16	0.05		

Table 6: Statistical Analysis of BET surface areas of non-grooved membranes, grooved membranes, and cotton

Analysis of Variance

Source	DF	Sum of Squares	Mean	F Ratio	Prob >
Extracted	2	1.005651	0.502825	44.243	0.0001*
Error	7	0.0795552	0.011365		
C. Total	9	1.0852062			

Wilcoxon / Kruskal-Wallis Tests (Rank Sums)

1-way Test, ChiSquare Approximation

ChiSquare	DF	Prob>ChiSq
7.8545	2	0.0197*

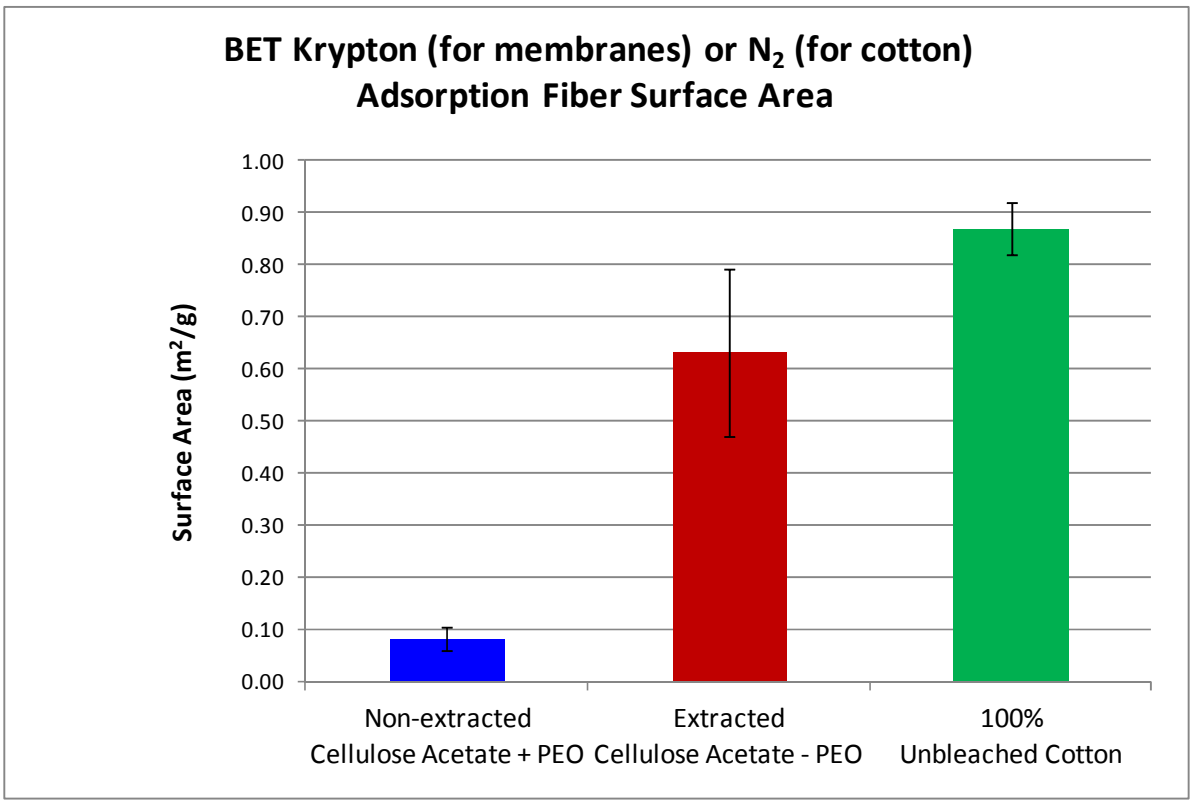

Figure 27: Experimental BET surface area of membranes and cotton

This increase in surface area for the grooved fibers was critical to achieve in order to test my hypotheses pertaining to an increased decontamination performance via increased fiber surface area for POM binding. It was surprising to see that cotton still had a higher surface area than the membranes, and this lead to the new hypothesis that the cotton would achieve the highest decontamination performance due to its available surface area for POM binding.

The large variability in the surface area result for the non-grooved fibers (standard deviation of 0.16) was most likely a result of the small sample sizes of the membranes that were tested and lack of uniformity of the fibers. Although all membranes were initially cut and measured to be the same dimensions as the cotton swatches, extraction caused the

membranes to shrink significantly leading to very small sample sizes of grooved membranes and less fiber uniformity.

7-2-4. Characterization of $H_5PV_2Mo_{10}O_{40}$ Grafted Cellulose Substrates

7-2-4-1. Fourier Transform Infrared Spectroscopy

When hexamethyl diisocyanate (HMDI) (liquid) was analyzed via FTIR, its absorption signature showed major peaks at 2260, 1660, 1160, 1040, 860, and 573 cm^{-1}. This spectrum of HMDI's functional groups as seen in Figure 28 (a) was similar to that of the POM powder Figure 28 (b); however, it was apparent that a peak at 2260 cm^{-1} was unique only for the HMDI. Examining the literature, it was found that nitrile groups can be identified from the FTIR spectrum in the triple bond region of 2300-2000 cm^{-1}. For isocyanates, a type of alkyl nitrile functional group, FTIR absorption bands are typically seen in the 2275-2240 cm^{-1} region of the spectrum. A peak at 2260 cm^{-1} or 2240 cm^{-1} correlates to the presence of a saturated alkyl nitrile (Robinson, 1991; Larkin et al., 2011). This peak at 2260 cm^{-1} was used as the reference peak to confirm the presence of the HMDI, and the resulting spectrum was used as a standard of comparison when analyzing the POM grafted electrospun membranes.

Figure 28 shows the FTIR absorbance spectrum of the POM powder standard (b), the 100% unbleached cotton standard (c), the unbleached 100% cotton swatch grafted with HMDI (d), and the unbleached 100% cotton swatch grafted with HMDI and the POM (e). Table 7 highlights the defining peaks for these five spectra and provides interpretations of the corresponding functional groups.

Table 7: FTIR spectral interpretation of grafting results

Sample	Wavenumbers of Interest (cm-1) Range 4000 - 550 cm^{-1}	Infrared Correlation Compound
Hexamethyl diisocyanate (HMDI) Control (liquid)	**2260**	isocyanate; saturated alkyl nitrile
$H_5PV_2Mo_{10}O_{40}$ (POM) (solid)	**1060**	vanadium oxide trigonal bipyramids, central phosphate tetrahedron, molybdenum oxide octahedra
	1160	central phosphate tetrahedron, hydrogen sulfate
Cotton (100%) Control (solid)	**1032**	secondary primary alcohol
60/40 CA/PEO Extracted membrane	**2879**	aliphatic ether
	1740	aliphatic acetate ester

As discussed in section 7-1-1, 1160 and 1060 cm^{-1} were chosen as the defining peaks for the molybdovanadate POM since these peaks corresponded well to the P-O, Mo-O, and V-O functional groups as well as the M-O-M vibrations (Nyquist and Kagel, 1971; Robinson, 1991; Misono and Okahura, 1993; Kozhevnikov, 1998; Zidan et al. 2000; Arichi et al., 2008; Arichi et al., 2010). Further evidence that the POM was present on the surface of the cotton and membranes included the presence of peaks and bands at 1650, 856, 768, and 600 cm^{-1} (Nyquist and Kagel, 1971; Robinson, 1991; Misono and Okahura, 1993; Kozhevnikov, 1998; Neumann, 1998; Popa et al., 2006; Arichi et al., 2008; Arichi et al., 2010; Larkin, 2011). The absence of a peak at 2260 cm^{-1} in the (e) spectrum of cotton grafted with POMs indicates that most HMDI, that was used as the grafting intermediate, reacted with the POM.

Table 8: Grafting results summary of FTIR spectra & absorbance peak heights

	Corresponding Figure	Sample	Wavenumbers of Interest (cm-1) Range 4000 - 550 cm^{-1}	Peak Height (Absorbance)
Additives		Hexamethyl diisocyanate (HMDI) Control (liquid)	**2260**	**0.138**
		$H_5PV_2Mo_{10}O_{40}$ (POM) (solid)	**1060**	**0.121**
			1160	**0.11**
Substrates		Cotton (100%) Control (solid)	**1032**	**0.155**
		60/40 CA/PEO Extracted membrane	**2879**	**0.017**
			1740	**0.120**
Grafting Results		Cotton + HMDI	**2260**	**0.044**
			1160	0.047
			1060	0.108
			1032	**0.127**
		Cotton + HMDI + POM	2260	0.009
			1160	**0.108**
			1060	**0.110**
			1032	**0.137**
		60/40 CA/PEO Extracted membrane + HMDI	**2879**	**0.025**
			2260	**0.034**
			1740	**0.161**
			1160	0.081
			1060	0.218
		60/40 CA/PEO Extracted membrane + HMDI + POM	**2879**	**0.085**
			2260	0.059
			1740	**0.070**
			1160	**0.177**
			1060	**0.185**

Bold = peak

The table of FTIR spectrum peak heights (Table 8) summarizes that the absorbance peak height of the HMDI band at 2260 cm^{-1} decreased from 0.044 for the HMDI grafted cotton to 0.009 for the POM grafted HMDI functionalized cotton. It was more difficult to detect this effect for the POM grafted membranes in Figure 28: (e) since the bands that resulted from the presence of the POM in the range of 2200-3600 cm^{-1} appear to have possibly coincided with the HMDI band at 2260 cm^{-1} . As a result, the absorbance peak height at 2260 cm^{-1} increased from 0.034 for the HMDI grafted membrane to 0.059 for the

POM grafted HMDI functionalized membrane. It is unlikely that this increase in peak height indicates an increase in the amount of HMDI on the surface of the membrane. It cannot be determined from this spectrum whether all HMDI was reacted with the POMs. However, the strong, broad bands seen at 1640, 2240, 3200, 3537, and 3590 cm^{-1} in the spectrum of the POM grafted HMDI functionalized membrane are likely to indicate residual lattice water commonly found in the structure of the POM (Moffat, 2001). This observation can be correlated with the presence of the bands at 1640, 2240, 3200, 3537, and 3590 cm^{-1} in the spectrum of the POM powder control.

An absorption band at 1032 cm^{-1}, which is indicative of the four secondary aliphatic alcohols of cellulose, in Figure 28 (c), (d), and (e) correlated with the presence of the cotton substrate. An absorption band at 2879 cm^{-1}, which is indicative of the aliphatic ether groups of polyethylene oxide, and a band at 1740 cm^{-1}, which is indicative of the acetate ester functional groups of cellulose acetate, in Figure 29 (a), (b), and (c) correlated with the presence of the 60/40 CA/PEO extracted membrane substrate.

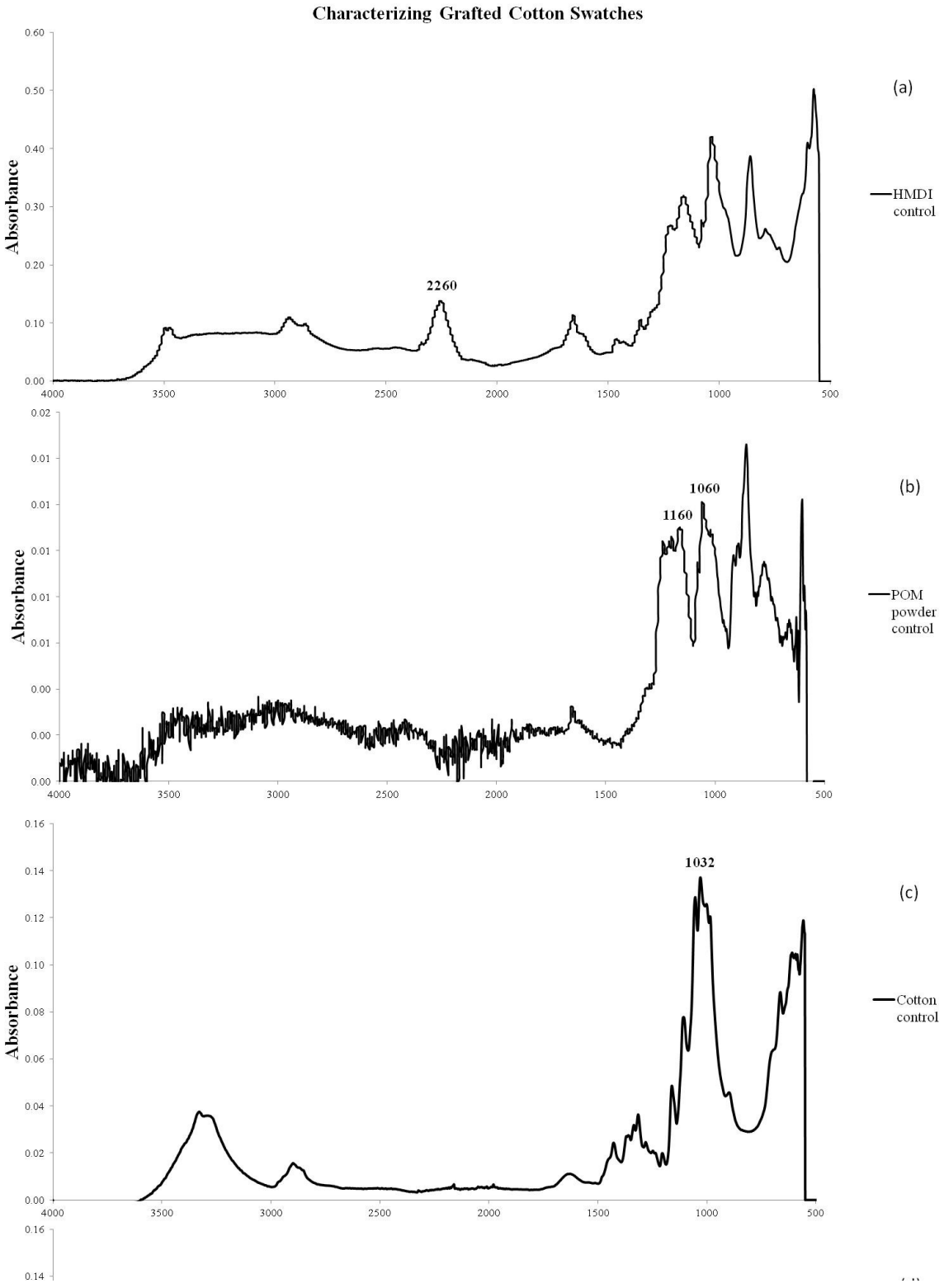
Characterizing Grafted Cotton Swatches
Absorbance
2260
(a)
HMDI control
1160
1060
(b)
POM powder control
1032
(c)
Cotton control

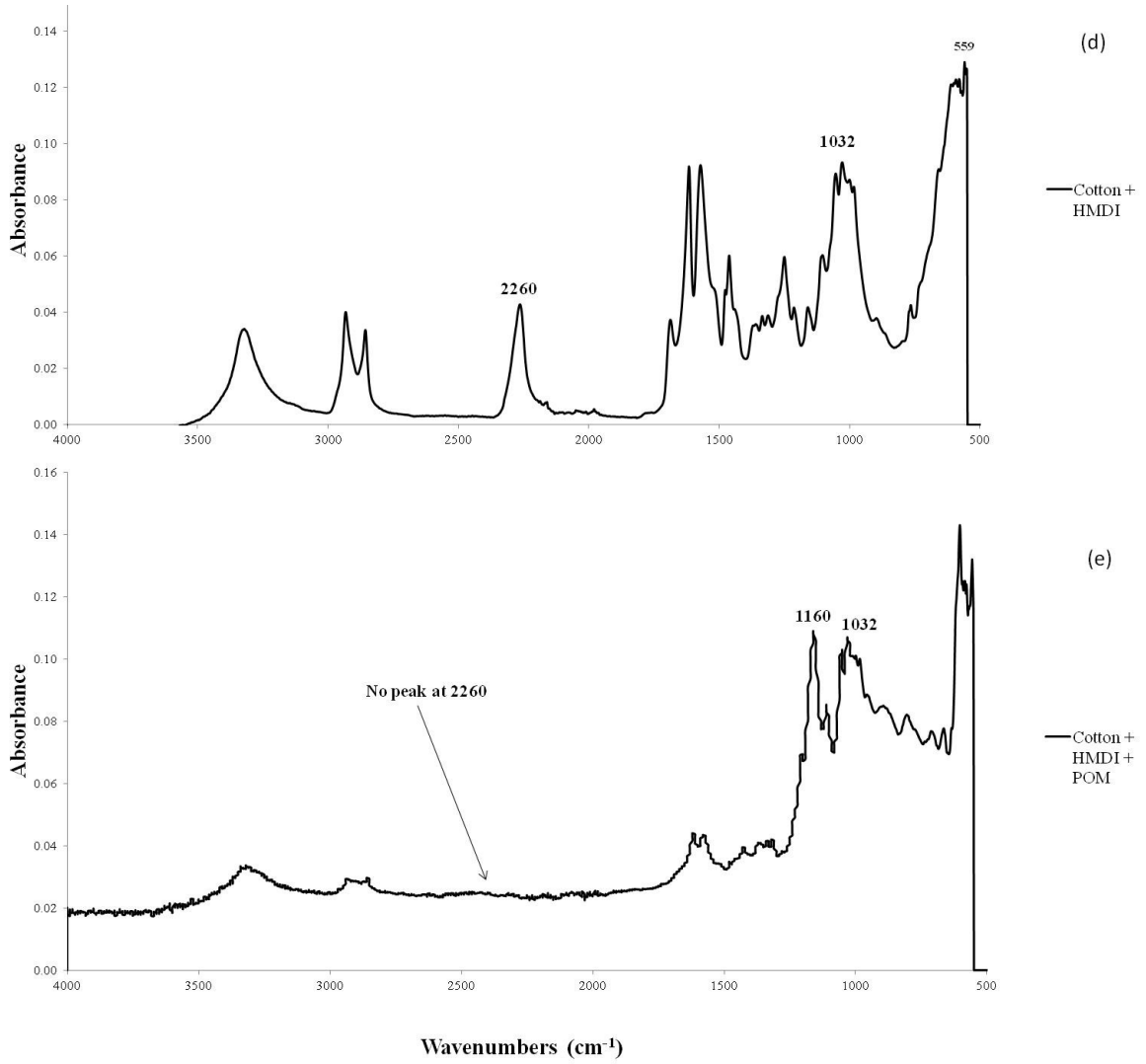

Figure 28: (a) FTIR of HMDI (liquid), (b) H5PV2Mo10O40 POM powder, (c) 100% Unbleached Cotton (d) 100% Unbleached Cotton + HMDI, (e) 100% Unbleached Cotton + HMDI + POM

It is important to note that the protocol for the grafting of the swatches and the membranes presented several issues that affected the grafting results and decontamination performance of the cotton swatches as well as the grooved and non-grooved membranes. The solvent in which grafting the HMDI and the POM took place was toluene, which was an excellent solvent for the HMDI since HMDI is moisture sensitive; however, the toluene

lead to considerable issues in the grafting of the POM. Due to the hydrophilicity of the POM, it had little affinity for the toluene and a greater affinity for the cotton swatch or membrane. This caused the POM not to disperse well in the grafting solution causing uneven distribution or leveling of the POM on the surface of the substrate. Subsequent washes in toluene following grafting, which should have removed any unreacted POM from the substrates did not succeed in removing unreacted POM since the POM still had a greater affinity for the substrate. Therefore, the FTIR spectrums that resulted from grafting are not representative of entirely grafted POM, but also of unreacted POM that was retained on the surface of the substrate.

In future work, using a grafting intermediate other than HMDI may allow for the grafting of the POM to take place in water, which would be a better solvent for even distribution and leveling of the POM on the surface of the substrates. Also, subsequent washes in water would act to remove the unreacted POM much more effectively that washes in toluene post-POM grafting.

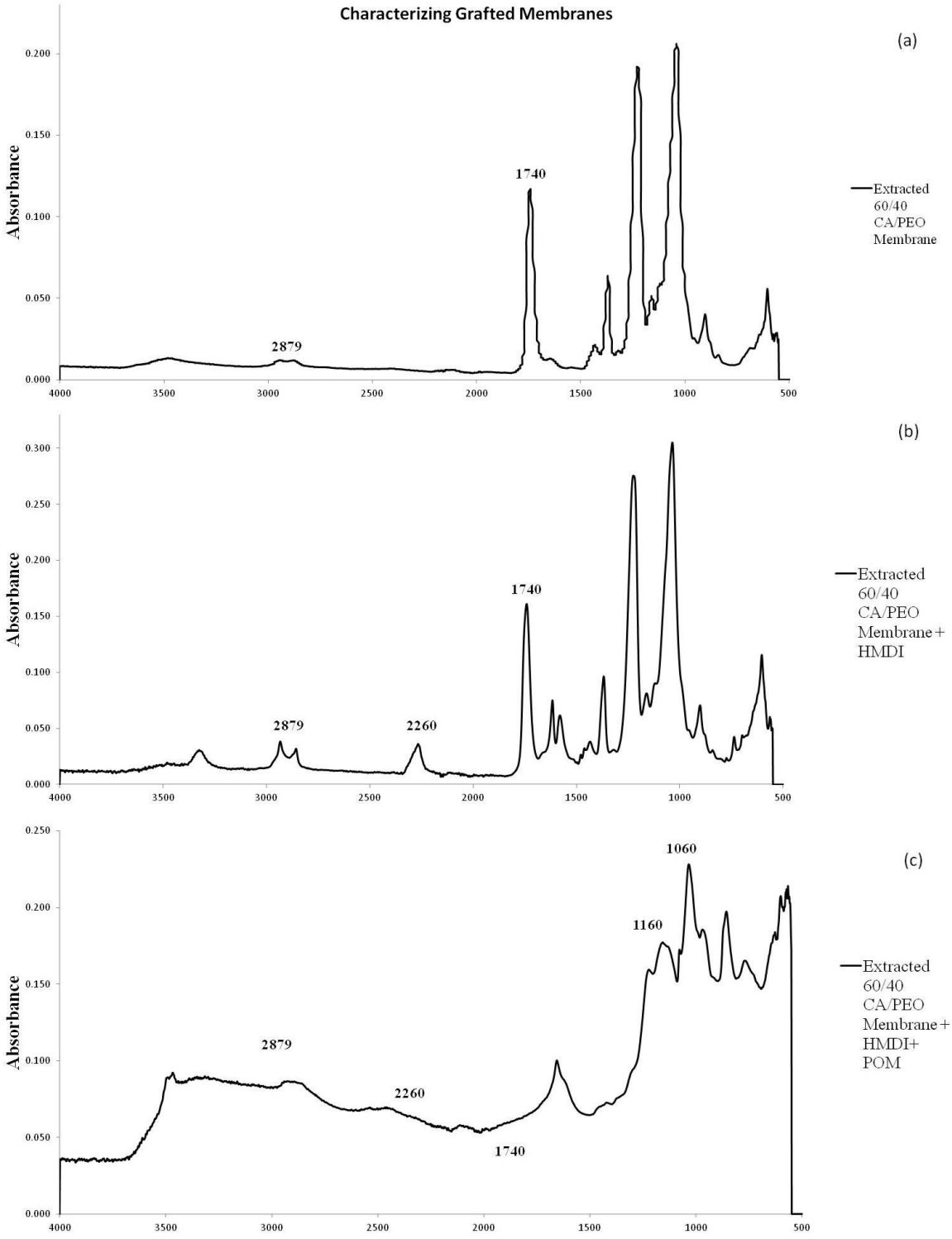

Figure 29: (a) Extracted 60/40 CA/PEO Membrane, (b) Extracted 60/40 CA/PEO Membrane + HMDI, (c) Extracted 60/40 CA/PEO Membrane + HMDI + POM

7-2-4-2. Thermogravimetric Analysis

While thermogravimetric analysis (TGA) can be a useful method for determining the percent content of some inorganic mixed-metal materials, it was not a good method for determining the percent add-on of the POM on the grooved and non-grooved membranes. It was expected that the thermal degradation curve after 750°C of the POM would indicate how much of the vanadium or molybdenum was present on the membrane and enable a quantitative analysis of the percent add-on of POM on the cotton or membrane substrate. The structure of $H_5PV_2Mo_{10}O_{40}$ is complex making the interpretation of the TGA thermal degradation somewhat difficult. Figure 30 shows the resulting thermal analysis of a known weight of POM grafted extracted membrane, a known weight of non-grafted extracted membrane, and a known weight of the POM particles alone.

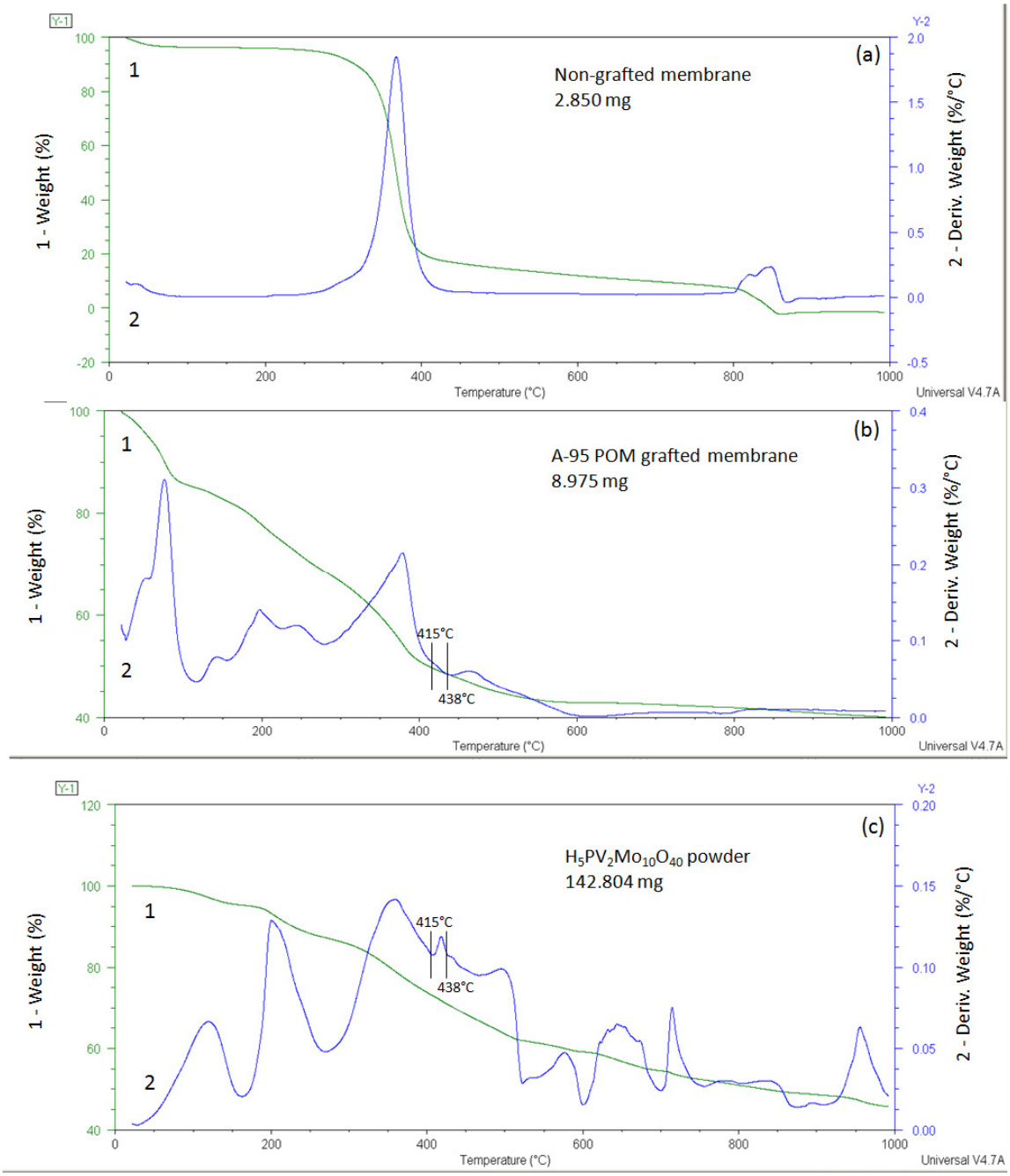

Figure 30: TGA of a non-POM+HMDI-grafted extracted membrane (a), a POM-grafted extracted membrane (b), and the POM itself in powder form (c)

Curve 1 in each of the graphs shows the decrease in weight percent of the tested compounds, while curve 2 calculates the derivative weight loss per degree centigrade. In

terms of the $H_5PV_2Mo_{10}O_{40}$ powder, curve 2 indicates an initial weight loss just under 200°C. This is normally indicative of dehydration of the compound. Further release of water and oxygen species (O_2/xH_2O, yO_2) appears to occur in the temperature range of 250-340°C. The crystallization of MoO_3 is generally associated with an exothermic peak at 418°C; however, the small endothermic peak at 415°C is more likely to indicate further water removal from the HPVMo compound. Molybdovanadates tend towards good thermal stability due to the presence of the vanadium complex and thus degradation of the Keggin unit of the POM is not expected to occur until the compound reaches temperatures greater than 500°C (Popa et al., 2006). A quantitative analysis of the percent add-on of the POM treated substrate is not possible since the weight analysis of the POM is below the detection limit of the TGA curve.

7-2-5. Decontamination of Methyl Parathion by POM/Cellulose Membrane

7-2-5-1. Reaction with Methyl Parathion and POM Grafted Substrates

No degradation of methyl parathion was observed when the toxin simulant was exposed to POM in powder form (5%, 10% and 20% POM w/v in MP/hexane solution). However, degradation of methyl parathion was observed when POMs were grafted to fibrous substrates. Figure 31 represents the decontamination performance of the POM grafted 60/40 CA:PEO grooved and non-grooved membranes. It shows that the grooved membranes with the higher surface area degrade significantly more methyl parathion than the non-grooved fibers. Using the equation derived from the calibration curve of methyl parathion, it was determined that the non-grooved fibers resulted in a 6.90% decrease in the concentration of methyl parathion present in the methyl parathion / hexane solution

while the grooved fibers resulted in a 12.85% decrease in the concentration of methyl parathion present in the methyl parathion / hexane solution. In terms of the amount of methyl parathion degraded by the POM, this translates to a decrease from 13.92 mg of methyl parathion in hexane solution to an amount of 12.96 mg of methyl parathion in the hexane solution as a result of POM grafted non-grooved fibers and 12.13 mg of methyl parathion in the hexane solution as a result of POM grafted grooved fibers. Therefore, the grooved fibers achieved twice the amount of methyl parathion degradation than the non-grooved fibers. Statistical analysis (Table 9) shows that the amount of degradation of methyl parathion by the grooved membranes was statistically significant with a p-value of 0.001. These results confirm my hypotheses that by using a high surface area substrate leads to an increase in POM binding sites that results in improved decontamination performance.

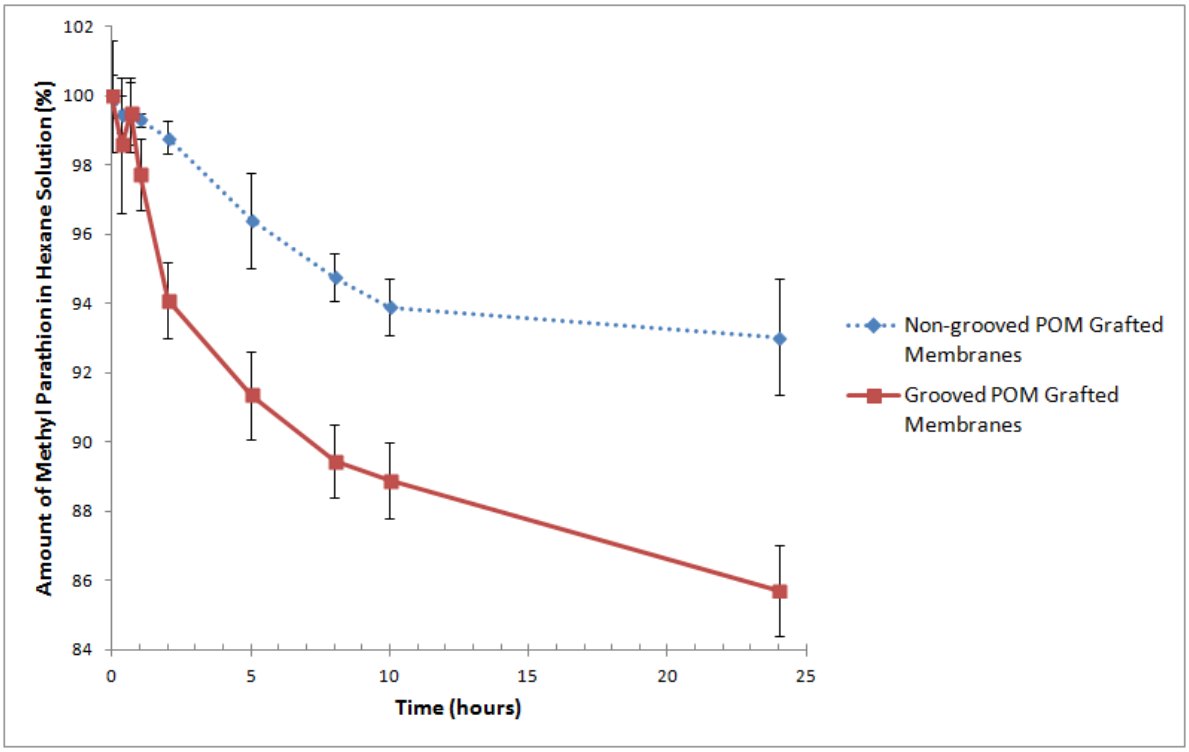

Figure 31: Degradation of methyl parathion by POM grafted membranes

Table 9: Repeated Measures ANOVA statistical analysis of methyl parathion degradation by POM grafted non-grooved membranes (A), POM grafted grooved membranes (B), and POM grafted cotton

Repeated Measures ANOVA

Term	Estimate	Std Error	DFDen	t Ratio	Prob>|t|
Intercept	94.861044	1.127785	60	84.11	<.0001*
Non-grooved POM-grafted Membranes	12.409719	1.125918	60	11.02	<.0001*
Grooved POM-grafted Membranes	9.0139382	1.125918	60	8.01	<.0001*
Time (hours)	-1.632396	0.103096	60	-15.83	<.0001*
[Non-grooved POM-grafted Membranes]*(Time (hours)-6.27182)	1.3203552	0.14191	60	9.3	<.0001*
[Grooved POM-grafted Membranes]*(Time (hours)-6.27182)	1.02797	0.14191	60	7.24	<.0001*

It is evident from Figure 32 that the POM grafted cotton degraded significantly more methyl parathion than either the grooved or non-grooved POM grafted fiber membranes. In terms of the decrease in methyl parathion concentration, the cotton

degraded the methyl parathion completely (100%) after 24 h; whereas, there was still methyl parathion present in the hexane solution after being exposed to the POM grafted membranes (grooved and non-grooved) for 24 h. The increased degradation by cotton may be due to more than simply its higher BET surface area, which was larger than both the surface area of the non-grooved and grooved fiber membranes. The degradation performance of cotton may also be due to the morphology of cellulose fibers in cotton.

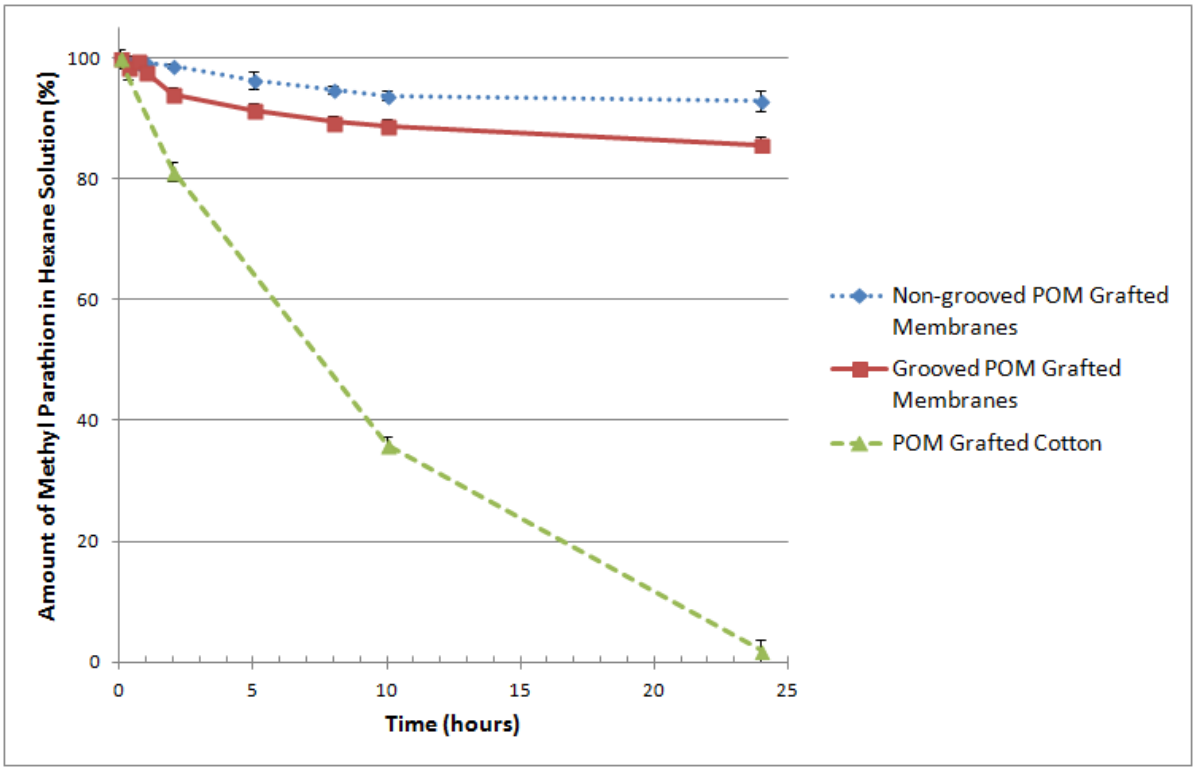

Figure 32: Degradation of methyl parathion by POM grafted membranes & POM grafted cotton

Cotton fibers have been extensively studied for their unique chemistry and morphology. They consist of six major parts that include the cuticle, the primary wall, a layer often referred to as the winding layer or S1, the multilayer secondary wall (S2), the lumen wall (S3), and the lumen. The cuticle is the outer layer composed of pectins and

waxes that is usually scoured away to create a finished textile and has little impact on the morphology of the cotton swatches used in the decontamination experiments. The primary wall is a thin cell wall composed of a network of fine cellulose fibrils. These fine fibrils also comprise a layer of very fine capillaries which are known for their ability to "rob liquids" from the course capillaries of the multilayer morphology (Rollins and Tripp, 1954). The S1 layer or "winding layer" is composed of microfibrils wound at a 40 to 70° angle to the fiber axis. The secondary wall or S2 has multiple concentric layers of cellulose strands wound at 70 to 80° angles to the fiber axis. The close packing of these fibrils and layers of fibrils form many micro capillaries that account for much of the liquid adsorption and absorption of cellulose (Hebert et al., 1970). The lumen wall (S3) is more chemically resistant to certain reagents than the primary or secondary walls and protects the lumen, which when the cotton plant is no longer alive, the lumen collapses forming a large pore or void in the center of the fiber. Figure 33 shows the main parts of the cotton fiber (Rollins and Tripp, 1954; Cotton, 2009).

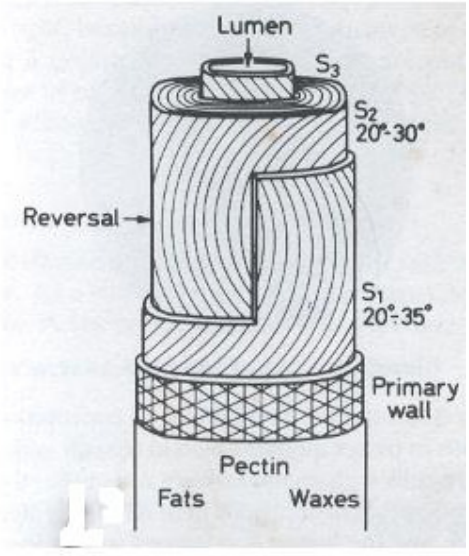

Figure 33: The structure of a cotton fiber (Rollins and Tripp, 1954)

Throughout the cotton fiber structure, these microfibrils of the multilayers form capillary spaces and pores in a range of sizes. These increase the capillary action of the fiber and make it very accessible to liquids and vapors, which can then be stored in the pores between fibrils. This fiber morphology and the hydrophilic chemical structure of cotton result in a high moisture regain of 7.1~8.5% and a moisture absorption of 7~8% (McCrea, 1924, Brandrup and Immergut, 1989). When the cotton fiber is viewed longitudinally, one can see that it is fibrillated on the end that was originally attached to the cotton seed and tapered at the other end. The middle portion is flat and ribbon-like with a twisted structure of 50 to 100 convolutions per inch (Cotton, 2009). This quality, as well as the high capillary porosity of cotton, give cotton highly unique absorbent qualities and explains why the BET nitrogen gas absorption value of cotton is 0.72 in the literature (Rowen and Blain, 1947). The BET nitrogen gas absorption value is significantly higher than that of cellulose acetate, which is 0.38 according to the literature, since the cellulose acetate fibers do not contain the same porous structure with microfibril, microcapillary morphology (Blair and McElroy, 1976).

Therefore, the morphology of cotton, containing a multitude of multi-size pores and capillary spaces where more POM particles could have become trapped, may also be contributing significantly to the increased degradation performance of methyl parathion. The high moisture regain and moisture absorption properties of cotton may also play a role in methyl parathion degradation. As discussed in section 4.1, the presence of water plays a significant role in POM catalytic oxidation in non-aqueous or non-polar environments such as the methyl parathion / hexane solution in which degradation testing was performed. It is known that as water content increases, the rate of catalytic oxidation by POMs such as

$H_5PV_2Mo_{10}O_{40}$ increases (Gall et al., 1994). Substrate samples were always vacuum dried prior to degradation testing. However, moisture from ambient air came into contact with the substrates when they were transferred into the degradation testing jars. Also, residual water in the lattice of the POM particles, as seen in the FTIR results, may have been absorbed by the substrates. Since cotton has higher moisture regain than cellulose acetate (6.5% moisture regain), it is possible that this higher water content in cotton enabled greater methyl parathion degradation via catalytic oxidation (Lewin and Pearce, 1998).

In examining other possible reasons for the complete methyl parathion degradation of the POM grafted cotton, it is important to consider mechanisms other than catalytic oxidation by which POMs can degrade organophosphates. It is possible that methyl parathion was degraded via hydrolysis, which could explain why cotton, having a higher moisture regain than the grooved cellulose acetate fiber membranes and non-grooved cellulose acetate / polyethylene oxide membranes, exhibited the highest amount of methyl parathion degradation (Fee, 2000; Metcalf, 2000; Morrow and Trogler, 1989). This could also explain why POM particles not in the presence of a textile substrate (see section 6-3-7-2-1) exhibited no degradation of methyl parathion. Without the presence of moisture in the textile substrates, it is possible that catalytic oxidation and/or hydrolysis of methyl parathion could not take place. Further testing of the residual moisture of the substrates and thermal analysis may provide insight into this possibility.

In summary, Figure 32 shows that $H_5PV_2Mo_{10}O_{40}$ degrades methyl parathion and suggests that the amount of decontamination is dependent on the substrate. A higher surface area substrate such as the grooved 60/40 CA:PEO fibers degrades more methyl parathion than a lower surface area substrate such as the non-grooved 60/40 CA:PEO

fibers; and the highest surface area substrate (the cotton specimen) degraded the most methyl parathion. In the case of cotton, the methyl parathion was degraded completely.

Regarding the degradation of methyl parathion and the expected degradation products of p-nitrophenol and methyl paraoxon, no peaks for degradation products were apparent in the HPLC-DAD results. For each degradation test the standard solution of p-nitrophenol in water showed a peak at 320 nm with a 5 min retention time, and the standard solution of methyl paraoxon in hexane showed a peak at 280 nm at a 5 min retention time. The standard solution of methyl parathion showed a peak at 320 nm with a retention time of 16 min. Over the time of degradation testing, the peak area of the methyl parathion decreased at the 16 min retention time; however, no peaks were apparent at 280 nm or 320 nm with 5 min retention times indicating that the expected degradation products were not present as the POM degraded methyl parathion over time. This may indicate that the POM completely mineralized methyl parathion and its degradation products. Degradation of methyl parathion by hydrolysis would have also produced the degradation product of p-nitrophenol and a second degradation product, diethylthiophosphate. If the expected degradation products were mineralized, ion chromatography could be used to further examine and quantify the degradation results of the POM.

7. Conclusions

The POM $H_5PV_2Mo_{10}O_{40}$ was synthesized as a non-crystalline precipitate to be used to functionalize fibers to obtain self-decontamination. The electrospinning of a 60/40 CA: PEO co-continuous fiber membrane creates non-grooved fiber morphology. By extracting the PEO from the membranes, grooved fiber morphology is created which has a surface area higher than the BET surface area of the non-grooved fibers.

The creation of the unique grooved fiber morphology led to an increase in the amount of surface area for the nanofibrous membranes. This increase in BET gas adsorption surface area of the membranes provided more fiber surface for POM binding. Twice as much methyl parathion degradation was observed for the grooved fibers than for the non-grooved.

Higher degradation was observed with cotton fabric treated with POM than the nanofibrous membrane. All of the methyl parathion was mineralized with the cotton-POM treated fabric. This self-decontamination performance is thought to be related to the fiber morphology of cotton and high moisture regain of cellulose.

8. Applications

POMs have been examined for applications in water and air filtration as well as protective apparel (Xu et al., 2000; Walker et al., 2003). POMs can be combined with other reactive compounds and incorporated into layered textile networks of chemically protective fabrics to decontaminate a range of hazardous chemical warfare agents on contact before CWAs are able to penetrate the fabric and reach the wearer's skin. POMs

can be incorporated on textile substrates in a number of ways such as grafting or electrostatic binding (Xu et al., 2000). The ability of POMs to "self-clean" not only offers the wearer protection from CWA penetration, but also decontaminates the fabric via toxin degradation so that the wearer can avoid contaminating surfaces and themselves when doffing the protective garment. Because POMs are catalytic and self-regenerate, these particles incorporated in a fabric could also provide reusable protective garments for both military applications and agriculture applications where workers are exposed to toxic pesticides. If the presence of moisture enhances the POM degradation of toxins, as suggested in the results of this study, this may make POMs more useful to incorporate in high moisture regain fabrics or in high humidity environments.

The moisture regain of the cellulose acetate grooved fibers could be improved by converting cellulose acetate into cellulose. Liu and Hsieh, 2002, illustrated that electrospun cellulose acetate nanofibers could be converted to cellulose nanofiber membranes via alkaline hydrolysis in a process known as deacetylation. In this process cellulose acetate fibers are treated with sodium hydroxide and ethanol over a specified period of time, washed, neutralized, and dried under vacuum. FTIR analysis can be performed in order to confirm the removal of the acetate group and the complete conversion of the cellulose acetate to cellulose fibers (Liu and Hsieh, 2002 and Dixit et al., 2009). Since the moisture regain of fabrics is closely linked to the perceived comfort of fabrics, the use of POMs in cellulose-based protective apparel may help bridge the gap between protection and comfort.

The results of this study show that complete degradation of methyl parathion occurred on the POM-grafted cotton after 24 h. (It is unknown how long it would take to

achieve complete POM degradation using the grooved or non-grooved fibrous membranes.) This amount of time for toxin degradation is too long for these particular POM grafted materials to be considered for protective apparel applications in defense or agriculture. Examining factors such as load dependence, the role of moisture, and the properties of textile substrates when treated with POMs, will help to determine how this rate of degradation may be accelerated in future studies. If the POM grafted fabrics of this study were scaled to a larger size, they could be useful as filtration media for industrial air or water purification applications that can allow for a greater amount of time for toxin degradation. As technologies with POMs continue to emerge, it will be important to assess the ramifications of human contact with POMs in order to understand their full range of potential as self-cleaning agents.

9. Works Consulted

1. (1993). Environmental Health Criteria 145, Methyl Parathion. *World Health Organization.* Retreived June 3, 2011, from http://www.inchem.org/documents/ehc/ehc/ehc145.htm.

2. Almond, M. (January 01, 1990). Fourier Transform Raman spectroscopy — a tool for inorganic, organometallic and solid state chemists?. *Spectrochimica Acta Part A: Molecular Spectroscopy, 46,* 2, 177-186.

3. Arichi, J., Eternot, M., & Louis, B. (October 15, 2008). Synthesis of V-containing Keggin polyoxometalates: Versatile catalysts for the synthesis of fine chemicals?. *Catalysis Today, 138,* 117-122.

4. Arichi, J., Louis, B., Pereira, M. M., & Esteves, P. M. (February 08, 2010). Synthesis of Keggin-type polyoxometalate crystals. *Solid State Sciences, 12,* 11, 1866-1869.

5. Brandrup, J., & Immergut, E. H. (1989). *Polymer handbook*. New York: Wiley.

6. Britt, D., Tranchemontagne, D., & Yaghi, O. M. (August 19, 2008). Metal-organic frameworks with high capacity and selectivity for harmful gases. *Proceedings of the National Academy of Sciences of the United States of America, 105,* 33, 11623-11627.

7. Cotton Fibre Morphology, Textile Information, (May 16, 2009). http://textileinformation.blogspot.com/2009/05/cotton-fibre-2-morphology.html (November 26, 2012).

8. Dimotakis, E. D., Cal, M. P., Economy, J., Rood, M. J., & Larson, S. M. (January 01, 1995). Chemically treated activated carbon cloths for removal of volatile organic carbons from gas streams: Evidence for enhanced physical adsorption. *Environmental Science & Technology, 29,* 7, 1876.

9. Dixit, V., Tewari, J., & Obendorf, S. K. (October 01, 2010). Fungal growth inhibition of regenerated cellulose nanofibrous membranes containing quillaja saponin. *Archives of Environmental Contamination and Toxicology, 59,* 3, 417-423.

10. Drechsler, U., Singh, W. and Sharma, A., (2009). *U.S. Patent Application No. 2009/0012204 A1.* Washington, DC: U.S. Patent and Trademark Office.

11. Doshi, J., & Reneker, D. H. (January 01, 1995). Electrospinning process and applications of electrospun fibers. *Journal of Electrostatics, 35,* 151.

12. Echlin, P. (2009). *Handbook of sample preparation for scanning electron microscopy and x-ray microanalysis*. New York: Springer.

13. Fee, Darrell C. (2000). "Phosphorus Compounds". *Kirk-Othmer Encyclopedia of Chemical Technology (0-471-48494-6, 978-0-471-48494-3)*. Hoboken, NJ, USA: John Wiley & Sons, Inc.

14. Fukumoto, K., Onoda, S., Sugiura, M., Horii, M., and Hayashi, H., (1997). *U.S. Patent No. 5,603,927.* Washington, DC: U.S. Patent and Trademark Office.

15. Gall, R. D., Faraj, M., & Hill, C. L. (January 01, 1994). Role of Water in Polyoxometalate-Catalyzed Oxidations in Nonaqueous Media. Scope, Kinetics, and Mechanism of Oxidation of Thioether Mustard (HD) Analogs by tert-Butyl Hydroperoxide Catalyzed by $H_5PV_2Mo_{10}O_{40}$. *Inorganic Chemistry, 33,* 22, 5015.

16. Gall, R., Hill, C., & Walker, J. (April 01, 1996). Selective Oxidation of Thioether Mustard (HD) Analogs by tert-Butylhydroperoxide Catalyzed by $H_5PV_2Mo_{10}O_{40}$ Supported on Porous Carbon Materials. *Journal of Catalysis, 159,* 2, 473.

17. Gall. R., Hill, C. L., & Walker, J. E. (January 01, 1996). Carbon Powder and Fiber-Supported Polyoxometalate Catalytic Materials. Preparation, Characterization, and Catalytic Oxidation of Dialkyl Sulfides as Mustard (HD) Analogues. *Chemistry of Materials: a Publication of the American Chemical Society, 8,* 10, 2523.

18. Goldstein, J. (1981). *Scanning electron microscopy and X-ray microanalysis: A text for biologists, materials scientists, and geologists*. New York: Plenum Press.

19. Gratton, L. M., Paglia, S., Scattaglia, F., & Cavallini, M. (May 01, 1978). Infrared Emission Spectroscopy Applied to the Oxidation of Molybdenum. *Applied Spectroscopy, 32,* 3, 310-316.

20. Hebert, J. J., Giardina, R., Mitcham, D., & Rollins, M. L. (February 01, 1970). The Effect of Convolutions on Orientation Measurements in Cotton Fibers. *Textile Research Journal, 40,* 2, 126-129.

21. Herguth, B. (March 2002). Grease Analysis - Monitoring Grease Servicability and Bearing Condition. *Machinery Lubrication,* http://www.machinerylubrication.com/Magazine/Issue/Practicing%20Oil%20Analysis/3/2002.

22. Hill, C. L., & Brown, R. B. (January 01, 1986). Sustained epoxidation of olefins by oxygen donors catalyzed by transition metal-substituted polyoxometalates, oxidatively resistant inorganic analogs of metalloporphyrins. *Journal of the American Chemical Society, 108,* 3, 536-8.

23. Hill, C., Duncan, D., & Harrup, M. (January 01, 1993). Multifunctional Polyoxometalates as Catalysts for Environmentally Benign Processes. *Comments on Inorganic Chemistry,14,* 6, 367-384.

24. Hill, C. L., & Prosser-McCartha, C. M. (January 01, 1995). Homogeneous catalysis by transition metal oxygen anion clusters. *Coordination Chemistry Reviews, 143,* 407.

25. Hill, C., Xu, L., Rhule, J. T., Boring, E., (2001). World Intellectual Property Organization No. WO 01/34279 A2, WPO Patent and Trademark Office.

26. Hong, S., Kim, J., Lemley, A. T., Obendorf, S. K., & Hedge, A. (January 01, 2001). Analytical method development for 18 pesticides in house dust and settled residues using SEC, SPE, TMS methylation, and GC-MS. *Journal of Chromatographic Science, 39,*3, 101-12.

27. Hug, S. J., Johnson, A., Friedl, G., Lichtensteiger, T., Belevi, H., & Sturm, M. (January 01, 1997). Characterization of Environmental Solids and Surfaces. *Chimia Zurich- , 51,* 12, 884-892.

28. Jeannin, Y. P. (January 01, 1998). The Nomenclature of Polyoxometalates: How To Connect a Name and a Structure. *Chemical Reviews, 98,* 1, 51.

29. Johnson, R. P., & Hill, C. L. (January 01, 1999). Polyoxometalate oxidation of chemical warfare agent simulants in fluorinated media. *Journal of Applied Toxicology: Jat, 19,* 71-5.

30. Keggin, J. F. (1933). Structure of the Molecule of 1,2-Phosphotungstic Acid. Structure of the Crystals of 1,2-Phosphotungstic Acid. *Nature, 351*, 908-909.

31. Khenkin, A. M., Weiner, L., Wang, Y., & Neumann, R. (January 01, 2001). Electron and oxygen transfer in polyoxometalate, $H_5PV_2Mo_{10}O_{40}$, catalyzed oxidation of aromatic and alkyl aromatic compounds: evidence for aerobic Mars-van Krevelen-type reactions in the liquid homogeneous phase. *Journal of the American Chemical Society, 123,* 35, 8531-42.

32. Kientz, C. E. (1998). Chromatography and mass spectrometry of chemical warfare agents, toxins and related compounds: State of the art and future prospects. *Journal of Chromatography a, 814*(1-2), 1-23.

33. Kozhevnikov, I. V., & Matveev, K. I. (January 01, 1983). Homogeneous catalysts based on heteropoly acids (review). *Applied Catalysis, 5,* 2, 135-150.

34. Kozhevnikov, I. K. (January 01, 1998). Catalysis by Heteropoly Acids and Multicomponent Polyoxometalates in Liquid-Phase Reactions. *Chemical Reviews, 98,* 1, 171-198.

35. Larkin, P. (2011). *Infrared and raman spectroscopy: Principles and spectral interpretation*. Amsterdam: Elsevier.

36. Lewin, M., & Pearce, E. M. (1998). *Handbook of fiber chemistry*. New York: Marcel Dekker

37. Liu, H., & Hsieh, Y.-L. (January 01, 2002). Ultrafine Fibrous Cellulose Membranes from Electrospinning of Cellulose Acetate. *Journal of Polymer Science. Part B, Polymer Physics, 40,* 18, 2119.

38. Ma, K., Chan, C. K., Liao, S., Ramakrishna, S., Hwang, W. Y. K., & Feng, Q. (May 01, 2008). Electrospun nanofiber scaffolds for rapid and rich capture of bone marrow-

derived hematopoietic stem cells. *Biomaterials,29,* 13, 2096-2103.

39. McCann, J. T.; Li, D.; Xia, Y. N. "Electrospinning of Nanofibers with Core-Sheath, Hollow, or Porous Structures" *J. Mater. Chem.* 2005, 15, 73.

40. Mansfield, E., Kar, A., Quinn, T. P., & Hooker, S. A. (December 15, 2010). Quartz crystal microbalances for microscale thermogravimetric analysis. *Analytical Chemistry, 82,* 24, 9977-9982.

41. McCrea, W. D. (1924). *An investigation of the rate of moisture regain in cotton yarns*.

42. Meek, G. A., & Elder, H. Y. (1977). *Analytical and quantitative methods in microscopy*. Cambridge: Cambridge University Press.

43. Metcalf, Robert L. (June 15, 2000). "Insect Control". *Ullmann's encyclopedia of industrial chemistry (3-527-30385-5, 978-3-527-30385-4).* Weinheim, Germany: Wiley-VCH Verlag GmbH & Co. KGaA.

44. Misono, M. (1987). Heterogeneous catalysis by heteropoly compounds of molybdenum and tungsten. *Catalysis Reviews Science and Engineering, 29*(2-3), 269-321.

45. Misono, M., & Okuhara, T. (November 01, 1993). Solid superacid catalysts. *Chemtech,*23-29.

46. Mizrahi, D. M., Saphier, S., & Columbus, I. (July 15, 2010). Efficient heterogeneous and environmentally friendly degradation of nerve agents on a tungsten-based POM.*Journal of Hazardous Materials, 179,* 1, 495.

47. Mizuno, N., & Misono, M. (1987). Pore structure and surface-area of $Cs_xH_{3-X}PM_{12}O_{40}$ (x=0-3, M=W, Mo). *Chemistry Letters,* (5), 967-970.

48. Moffat, J. B. (2001). *Metal-oxygen clusters: The surface and catalytic properties of heteropoly oxometalates*. New York: Kluwer Academic/Plenum Publishers.

49. Morrow, J. R., & Trogler, W. C. (June 01, 1989). Hydrolysis of phosphate triesters with copper(II) catalysts. *Inorganic Chemistry, 28,* 12, 2330-2333.

50. Muller, A., & Roy, S. (January 01, 2003). En route from the mystery of molybdenum blue via related manipulatable building blocks to aspects of materials science. *Coordination Chemistry Reviews, 245,* 1, 153.

51. Nakamoto, K. (1986). *Infrared and Raman spectra of inorganic and coordination compounds*. New York: Wiley.

52. Neumann, R., & Assael, I. (January 01, 1988). Oxybromination catalysed by the heteropolyanion compound H5PMo10V2O40 in an organic medium: selective para-bromination of phenol. *Journal of the Chemical Society, Chemical Communications,* 19, 1285-1287.

53. Neumann, R. (1998). Polyoxometalate complexes in organic oxidation chemistry. Progress in Inorganic Chemistry, 47, 317-370.

54. Nielsen, U. G., McKenzie, C. J., Hazell, A., Skibsted, J., & Jakobsen, H. J. (October 01, 2010). Solid-state ^{51}V MAS NMR spectroscopy determines component concentration and crystal phase in co-crystallised mixtures of vanadium complexes.*Crystengcomm, 12,* 10, 2826-2834.

55. Nguyen, L.; Mighri, F.; Deyrail, Y.;Elkoun, S. "Conductive Materials for Proton Exchange Membrane Fuel Cell Bipolar Plates Made from PVDF, PET and Co-continuous PVDF/PET Filled with Carbon Additives " *Fuel Cells* 2010, 10, 938.

56. Nyquist, R. A., & Kagel, R. O. (1971). *Infrared spectra of inorganic compounds (3800-45cm... [to the minus one])*. New York: Academic Press.

57. Ozer, R. R., and Ferry, J. L. (2000). Kinetic probes of the mechanism of polyoxometalate-mediated photocatalytic oxidation of chlorinated organics. *Journal of Physical Chemistry B, 104*(40), 9444-9448.

58. Pettersson, L., Andersson, I., Selling, A., & Grate, J. H. (January 01, 1994). Multicomponent Polyanions. 46. Characterization of the Isomeric Keggin Decamolybdodivanadophosphate Ions in Aqueous Solution by ^{31}P and ^{51}V NMR. *Inorganic Chemistry, 33,* 5, 982

59. Gibson, P., Schreuder-Gibson, H., Stote, R., Roylance, M., Capone, C., & Nakagawa, M., (1970). *Effect of Nanofibers on Spore Penetration and Lunar Dust Filtration*. INDA, Association of the Nonwovens Fabrics Industry.

60. Popa, A., Sasca, V., Stefanescu, M., Kis, E., & Marinkovic-Neducin, R. (January 01, 2006). The influence of the nature and textural properties of different supports on the thermal behavior of Keggin type heteropolyacids. *Journal of the Serbian Chemical Society, 71,* 3, 235-249.

61. Pope, M. T. (1983). *Heteropoly and isopoly oxometalates*. Berlin: Springer-Verlag.

62. Quantachrome Instruments. http://www.jazdlifesciences.com/pharmatech/research/Quantachrome-Instruments.htm?contentSetId=33963&supplierId=30000470. Accessed November 2, 2012.

63. Ramesh, S., Yuen, T. F., & Shen, C. J. (February 01, 2008). Conductivity and FTIR studies on PEO–LiX [X: CF3SO3−, SO42−] polymer electrolytes. *Spectrochimica Acta Part A: Molecular and Biomolecular Spectroscopy, 69,* 2, 670-675.

64. Ramirez, R., Casal, B., Utrera, L., & Ruiz-Hitzky, E. (December 01, 1990). Oxygen reactivity in vanadium pentoxide: Electronic structure and infrared spectroscopy studies.*Journal of Physical Chemistry,* 8960-8965.

65. Rao, C. N. R., Müller, A., & Cheetham, A. K. (2004). *The chemistry of nanomaterials: Synthesis, properties and applications in 2 volumes*. Weinheim: Wiley-VCH.

66. Robinson, J. W. (1991). *Practical handbook of spectroscopy*. Boca Raton: CRC Press. 526.

67. Rollins, M. L., & Tripp, V. W. (April 01, 1954). Optical and Electron Microscopic Studies of Cotton Fiber Structure. *Textile Research Journal, 24,* 4, 345-357.

68. Schreuder-Gibson, H., Gibson, P., Senecal, K., Sennett, M., Walker, J., Yeomans, W., Ziegler, D., Tsai, P. P. (January 01, 2002). Protective Textile Materials Based on Electrospun Nanofibers. *Journal of Advanced Materials, 34,* 3, 44.

69. Seger, M. R., & Maciel, G. E. (January 01, 2006). NMR investigation of the behavior of an organothiophosphate pesticide, methyl parathion, sorbed on clays. *Environmental Science & Technology, 40,* 2, 552-8.

70. Selim, H. M. E., & Sparks, D. L. (2001). *Heavy metals release in soils*. Boca Raton, Fla: Lewis Publishers.

71. Selling, A., Andersson, I., Pettersson, L., & Schramm, C. M. (January 01, 1994). Multicomponent Polyanions. 47. The Aqueous Vanadophosphate System. *Inorganic Chemistry, 33,* 14, 3141.

72. Senthilnathan, J., & Philip, L. (July 01, 2010). Removal of mixed pesticides from drinking water system using surfactant-assisted nano-TiO_2. *Water, Air, and Soil Pollution, 210,* 143-154.

73. Sharmila, M., Ramanand, K., & Sethunathan, N. (January 01, 1989). Hydrolysis of methyl parathion in a flooded soil. *Bulletin of Environmental Contamination and Toxicology, 43,* 1, 45-51.

74. Smith, B. C. (2011). *Fundamentals of Fourier transform infrared spectroscopy*. Boca Raton, FL: CRC Press.

75. Socrates, G. (1980). *Infrared characteristic group frequencies*. Chichester: Wiley.

76. Tan, K., & Obendorf, S. K. (January 01, 2006). Surface modification of microporous polyurethane membrane with poly(ethylene glycol) to develop a novel membrane.*Journal of Membrane Science, 274,* 1, 150.

77. Tan, K., & Obendorf, S. K. (January 01, 2008). Fabrication and evaluation of electrospun nanofibrous antimicrobial nylon 6 membranes. *Journal of Membrane Science, 305,*1, 287.

78. Tang, C.; Chen, P.; Liu, H. "Cocontinuous cellulose acetate/polyurethane composite nanofiber fabricated through electrospinning" *Polym. Eng. Sci*. 2008, 48, 1296.

79. Tian, J., Wang, J., Zhao, S., Jiang, C., Zhang, X., & Wang, X. (January 01, 2010). Hydrolysis of cellulose by the heteropoly acid $H_3PW_{12}O_{40}$. *Cellulose, 17,* 3, 587-594.

80. Tranchemontagne, D. J., Hunt, J. R., & Yaghi, O. M. (September 01, 2008). Room temperature synthesis of metal-organic frameworks: MOF-5, MOF-74, MOF-177, MOF-199, and IRMOF-0. *Tetrahedron, 64,* 36, 8553-8557.

81. Tsigdinos, G. A., & Hallada, C. J. (March 01, 1968). Molybdovanadophosphoric acids and their salts. I. Investigation of methods of preparation and characterization. *Inorganic Chemistry, 7,* 3, 437-441.

82. Vallejos, M. E., Peresin, M. S., & Rojas, O. J. (August 01, 2012). All-Cellulose Composite Fibers Obtained by Electrospinning Dispersions of Cellulose Acetate and Cellulose Nanocrystals. *Journal of Polymers and the Environment,* 2.)

83. Walker, J., Schreuder-Gibson, H., Yeomans, W., Ball, D., Hoskin, F., and Hill, C. , ARMY NATICK SOLDIER CENTER MA. (2003). *Development of self-detoxifying materials for chemical protective clothing.* Ft. Belvoir: Defense Technical Information Center.

84. Weinstock, I. A., Cowan, J. J., Barbuzzi, E. M. G., Zeng, H., & Hill, C. L. (May 01, 1999). Equilibria between α and β isomers of Keggin heteropolytungstates.*Journal of the American Chemical Society, 121,* 19.)

85. Woo, D.J., Unpublished Ph.D. Thesis, Cornell University (2012)

86. Wu, K. H., Yu, P. Y., Yang, C. C., Wang, G. P., & Chao, C. M. (September 01, 2009). Preparation and characterization of polyoxometalate-modified poly(vinyl alcohol)/polyethyleneimine hybrids as a chemical and biological self-detoxifying material. *Polymer Degradation and Stability, 94,* 9, 1411-1418

87. Xu, L., Boring, E., & Hill, C. (January 01, 2000). Polyoxometalate-Modified Fabrics: New Catalytic Materials for Low-Temperature Aerobic Oxidation. *Journal of Catalysis, 195,* 2, 394-405.

88. Zhang, R., Yang, C., & 5th. (January 01, 2008). Synthesis and Preparation of Novel Polyoxometalate-Functionalized Mesoporous Hybrid Materials.

89. Zhang, W.; Yao, D.; Zhang, Q.; Zhou, J. G.; Lelkes, P. I. "Fabrication of interconnected microporous biomaterials with high hydroxyapatite nanoparticle loading" Biofabrication 2010, 2, 1.

90. Zidan, M. D., & Allaf, A. W. (January 01, 2000). The gas-phase on-line production of vanadium oxytrihalides, VOX_3 and their identification by infrared spectroscopy.*Spectrochimica Acta. Part A, Molecular and Biomolecular Spectroscopy, 56,* 14, 2693-8.